Republic of Iraq
Ministry of Higher Education
& Scientific Research
University of Babylon
College of Education for Pure Sciences
Department of Physics

Study of Electron-Nucleus Scattering in sdpf Model Space for Some Deformed Nuclei

A Thesis

Submitted to the Council of the College of Education for Pure Sciences of University of Babylon in Partial Fulfillment of the Requirements for the Degree of Master in Education / Physics

By

Mohammed Layth Adnan Mohammed Jawad

B.Sc. In Physics, University of Babylon (2019)

Supervised by

Prof. Khalid S. Jassim, Ph.D.

College of Education for Pure Sciences

Department of Physics

2022 A.D. **1444 A.H.**

بِسْمِ اللَّهِ الرَّحْمَنِ الرَّحِيمِ

﴿ فَسُبْحَانَ الَّذِي بِيَدِهِ مَلَكُوتُ كُلِّ شَيْءٍ وَإِلَيْهِ تُرْجَعُونَ ﴾

صَدَقَ اللهُ العلِيُّ العظِيمُ

(سورة يس/ آية ٨٣)

Dedication

To my great, beloved and merciful mother for her support and encouragement.

To my dear family, all my thanks.

To my supporting friends.

Acknowledgments

First of all, Praise is to Allah, Mercy and peace are to the Prophet Mohammed and his relatives and companions.
I would like to sincerely thank my supervisor Prof. Dr. Khalid Salih Jassim for his direction, assistance, guidance, and his recommendations and suggestions for this work.
I am deeply indebted to the head of the Department of Physics, the staff and the dean of the College of Education for Pure Sciences for the support that provided.
I wish to express my thanks to all my friends, especially the master group for their kind assistance and support during our course study and thesis work.

Abstract

The longitudinal electron scattering form factors have been calculated for some light nuclei as ^{31}P, ^{23}Na, ^{27}Al and ^{25}Mg lies in the sdpf-shell region. The core is taken at ^{16}O nucleus. The shell model calculations, were performed by Nushell code for windows. The core-polarization effect is taken into account for all nuclei.

Bohr-Mottelson (BM) collective model is employed to calculate the electron scattering form factors with Harmonic oscillator (HO), Wood-Saxon's (WS), and Skyrme-Hartree (SKX) as the potentials.

The sdpf-space was used with sdpfnow residual effective interaction to calculate the eigenvalue and eigenvectors that used to calculate the one body density matrix (OBDM) to be used in the calculations of the inelastic and elastic electron scattering.

The experimental data are compared to the estimated inelastic and elastic electron scattering for the nuclei under study. The influence of core polarization through effective proton and neutron charges is shown to be highly important to include, and its agreement with experimental evidence for the Coulomb C0, C2, and C4 form factors significantly. The calculations with HO potential agreement with the experimental data for ^{23}Na nucleus, but SKX and WS potentials better than HO potential for ^{31}P, ^{27}Al and ^{25}Mg nuclei.

Contents

List of Figures

List of Tables

list of symbol and abbreviations

Symbol or Abbreviation	Meaning
TBME	Two body matrix element
$\hbar$	Planck constant reducer
ψ	Wave function
k	Electron wave number
λ	Wavelength
PWBA	Plane Wave Born approximation
DWBA	Distributed Wave Born approximation
Ze	Charge of nuclear
c	Speed of light
M3Y	Michigan three range Yukawa
$\frac{d\sigma}{d\Omega}$	Differential cross section for the scattering
CDD	charge density difference
σ_M	Mott cross section
α	Fine structure constant
E_i	Energy of incident electron
f_{rec}	The recoil factor of the nucleus
ω	The energy transfer
q	Three momentum transfer
q_μ	Four-momentum transfer
$F_J^\eta(q)$	(Longitudinal and Transverse) form factor
J	Total angular momentum
T	Total isospin
T_z	Projection isospin
m_o	The rest mass of the electron
b	Size parameter for HO
L	Orbital angular momentum quantum number
OBDM	One-body density matrix
$\left\{ \begin{array}{c} .... \\ .... \\ .... \end{array} \right\}$	9j-symbols
$\left(\begin{array}{c} .... \\ .... \end{array} \right)$	3j-symbols
$\hat{\rho}(\vec{r}, t_z)$	Nucleon charge density operator
$\hat{T}_{J,t_z}$	The longitudinal operator

$j_J(qr)$	Spherical Bessel function
$Y_{JM}(\Omega)_r$	Spherical harmonic function
$\delta(\vec{r}-\vec{r_i})$	Dirac delta function
$F_{c.m}(q)$	Center of mass form factor
$F_{f.s}(q)$	Form factor due to the nucleon-finite size
$\mathrm{d}\Omega$	Solid angle
Ω	Angular frequency
H	Hamiltonian
A	Mass number of nucleus
Z	Atomic number of the nucleus
CP	Core polarization
USDA	Universal sd-shell interaction A
MS	Model space
Γ	Gamma function
$F(a;b;y)$	The confluent hyper-geometric function
ρ_{Jt_z}	The transition charge density
q_{eff}	Effective momentum transfer
(rms)	The root mean square
B(CJ)	Reduced transition probability
$R_{nl}(r)$	Radial part of the single-particle wave function
C2,C4	Longitudinal Coulomb form factor for J=2 and J=4
SKx	SKyrme-Hartree Fock potential
HO	Harmonic oscillator
WS	Wood-Saxon
∇^2	Laplace operator
B(WL)	reduced transition probabilities
FB	Fourier-Bessel expansion
SOG	Sum of Gaussians expansion

Chapter One
General Introduction

1.1 Introduction

The shell model is the most important theoretical tool for understanding nucleus characteristics. It can provided qualitative insight in its most basic single particle form, but it can also be utilized as a foundation for far more complicated and comprehensive calculations. Soon, the application's expansion appears to be constrained[1]. The shell model occupies a prominent role because it is a more fundamental framework based on a smaller number of assumptions, as well as the fact that it has proved exceedingly successful in describing the nuclei at low excitation energies[2].

The shell model is consistent with quantum mechanics as well as with the Pauli exclusion principle. There are a variety of potentials that may be used to apply the nuclear shell model, including the infinite-dimension potential, the Harmoic oscillator (HO) potential, the Wood-Saxons (WS) potential, the Skyrme-Hartree (SKX) potential and many more potentials[3].

Measured static moments or transition strength cannot be reproduced without form factors in the nucleons' orbits in the Model space (MS). The nuclear shell model calculation was done. The necessity to scale the one-body operator matrix elements by effective charge to match the experimental data reveals shortcomings in the wave function. It's feasible that adding an effective charge will bring the anticipated photon point transition intensities and maximum form factors closer to the actual values. Nonetheless, the observed and non-zero momentum transfer values may differ dramatically[4].

There are certain phenomenological aspects to theoretical solutions to the nuclear many-body problem; as a result, theory and experiment are tightly linked. The actual example is the nuclear shell model, which serves as a framework for the models and their criteria[5]. The nuclear experiment relies on theory to assist choose the most significant tests to support or reject model predictions. It is common practice to utilize codes for nuclear shell models like OXBASH[6] and

MSHELL[7] across the world, other common codes are ANTOINE[8]; RETSSCHIL[9]; NATHAN[10]; NUSHELL[11]; and NUSHELL@MSU[12].

The shell model interactions based on two-body interaction strengths has been presented, with fitting parameters derived from basic nuclear interactions and the correct process. In order to two body matrix elements (TBME) is required [13], three sorts of nuclei may be identified in the shell model:
1-Closed-shell nuclei: The nuclei that have a totally filled shell and an empty outer shell.These nuclei contain the number of protons or neutrons or protons and neutrons equal to the magic numbers.
2-Only one of the shells contains a single particle, which represents the lowest level above the full core.
3-Nuclei with a full shell except for one incompletely filled shell require a single nucleon, which are referred to as single hole nuclei.
The nucleons in the shell that follow the inner shell are called valence nucleons, and the closed-shell is similar to the inactive nucleus. The valence shell refers to the outermost layer of that shell[14].

The scattering of electrons from nuclei can provide the most exact data on nuclear size and charge distribution. Electron scattering is a powerful and effective tool for analyzing nucleus structure[15]. Electrons scattering is used as a probe for a variety of reasons. The first is the electron-nucleus interaction with electromagnetic interactions, which is the most well-known interaction and is accurately described by quantum electrodynamics (QED). Second, the interaction between the electron and the nucleus is so weak that it does not greatly affect the structure of the nucleus. In addition, Within the one-photon exchange approximation, the interaction's weakness allows one to operate in first-order perturbation[16].

The high-energy scattering of electrons results in vital knowledge and important information about the nucleus. The size of the wavelength of de Broglie associated with the electron as compared to the range of nuclear forces determines the knowledge acquired from high energy electron scattering by nuclei. When the incoming electron's en-

ergy is in the range of 100 MeV or more, the de Broglie wavelength is in the range of the nucleus spatial extension. As a result, the electron is an ideal probe for probing nuclear structures with this energy.[17].

Calculations using the Born approximation should be done for those light elements that are available as acceptable experimental targets and are based on shell-model wave functions. Efforts to create convincing theories for heavy nuclei have progressed significantly and should be pursued further. It was clear that the improved concepts would require a significant amount of processing power[18]. It would be necessary for professionals to change the theories and calculations to be attached to carry out an efficient program with minimal duplication of effort.

Mott was the first to derive the scattering cross-section, which explained electron scattering and included the influence of electron spin. The "Nuclear form factor," which is determined by the ratio of the measured cross-section to the Mott cross-section, the nuclear form factor is dependent on the charge and magnetization distribution in the target nuclei. By knowing the energies of the incident and scattering electrons, as well as the scattering angle, the form factors may be calculated experimentally as a function of the momentum transfer (q)[19].

There are two types of electron scattering: The first is electron elastic scattering, which investigates ground state features such as static charge distribution and magnetic polarization, that occurs when the electron scatters from the nucleus and leaves it in the ground state without any change in energy between the incident electron and the scattering electron. The transition densities are determined by the second type, inelastic electron scattering, that occurs when the electron scatters from the nucleus and leaves it in the excited state with a difference in energy between the incident electron and the scattering electron.

Over the last fifty years, several nuclear models have been implemented. The nuclear shell model, which proved highly successful in explaining the nuclear structure, is one of these nuclear models[20]. By splitting nuclei into closed shells and valence nucleons, two techniques

for theoretical nuclear models are utilized to predict nuclei behavior. One method relies on a microscopic perspective of the mobility of individual nucleus particles and the residual interaction between them. Due to the enormous number of nucleon interactions, this model becomes intractable as the number of valence nucleons increases[21]. Instead, a different strategy is adopted, which is based on the global behavior of the nucleus. The simplest collective model, the semi-classical liquid drop model, is widely used as a starting point for simulating the nucleus at the microscopic level; in this model, the nucleus acts as a drop of liquid, held together by the nucleus attracting each other. This model has been expanded to include quantum mechanical collective motions like rotation and vibrations, resulting in the Bohr and Mottelson collective mode[21]. The nucleus in the collective model can rotate, vibrate, or show both types of movement.

Electron scattering cross-section theoretical calculation for various form factors, multi-pole transition probability, etc. Can all be found from electron scattering. Wave functions derived from Schrodinger's differential equation, such as HO potential energy functions, WS potential, and SKX potential are used in the calculation of nuclear shell model wave functions[22].

The charge density difference (CDD), transition densities, and form factors are all essential properties of nuclei that may be measured empirically via high-energy electron scattering. The more momentum transmitted to the nucleus, the more precise the data collected in these studies. The extended model space calculation combine all possible ways to distribute the nucleons to the available single-particle orbits that are significant in regions of light nuclei. The "model space" indicates the orbitals and the truncation within that set of orbitals assumed for a given calculation. Generally, the best and most complete results are obtained when the model space is as large as possible. However, the computation time increases exponentially with the size of the model space, and empirical Hamiltonians are better determined in smaller model spaces. The specific distribution of valance particles over a given set of valence orbits will be called a partition. The complete or "full" model space

includes all possible partitions for a given set of orbits. According to the fact that the space model represents considered orbitals in the calculations, considering the number of valence nucleons of Phosphorous (A=31), Sodium (A=23), Aluminum (A=27) and Magnesium (A=25), the appropriate model for performing the calculations for this nuclei are sdpf model space.

1.2 Literature Survey

Odd-even nucleus structure (or even-odd nucleus structure) and even-even has been studied extensively, and one may evaluate these studies about the current work:

A. A. Al-saad,(2012)[23], calculated the C2 transitions of longitudinal form factors in many states of ^{7}Li and ^{15}Na nuclei in a large extended space with include admixture from higher multi-$\hbar\omega$. He was able to find convergence between the experimental results and the obtained results.

To account for higher energy configurations beyond the sd–shell model space, K. S. Jassim and H. A. Kassim (2013)[24] explored inelastic electron scattering form factors in several odd-A sd-shell nuclei ^{17}O,^{27}Al, and ^{39}K. The sd-shell model space makes advantage of the Wildenthal interaction between two bodies. Researchers have studied the OBDM elements for the longitudinal C2 and C4 transition for ^{27}Al nucleus and the CP matrix elements interact is taken into account through first order perturbation theory via the (M3Y) interaction. Sd-shell model calculations cannot adequately describe both the transition strength and the form factor; however, when CP effects are taken into account, the form factor is dramatically altered, and the experimental data can be accurately described in terms of both the absolute strength and the dependence on the q.

Inelastic electron scattering in the ^{13}C nucleus is studied by N. Adeeb *et al.* (2013)[25]. They studied the $^{-}$3/2 1/2 (3.68 MeV), $^{-}$5/2 1/2 (7.55 MeV), and $^{-}$3/2 1/2 (15.11) MeV states. The nine nucleons outer the core and the ^{4}He makeup are inert (the model space of the

nucleus). Using Cohen-Kurath interaction for 1p-shell model space and MSDI as a residual interaction for higher configurations, form factors are determined. When studying the effects of CP on the form factors, the microscopic theory is used, which combines shell model wave function and configurations for the single-particle matrix elements. The oscillator's length parameter b is chosen to reproduce the nucleus's measured root mean square charge radius. The experimental data are well-aligned when the CP effects are taken into account.

R.A.Rahhi *et al.* (2014)[26], investigated elastic electron scattering form factors for ^{19}C nucleus by using Harmonic Oscillator(HO) as potential while they found that the total form factors of stable ^{13}C nucleus (non-halo) have the same behavior as the calculated form factors of exotic ^{19}C nucleus (halo) through Plane Wave Born Approximation (PWBA), but they differ in magnitude.

Some nuclei in fp-shell were studied by K. S. Jassim and Z. M. Abdul-Hamza (2014)[27]. They used the GXPF1 interaction Tassie model to calculate the Core-Polarization effects for $^{42-44,48}Ca$, $^{46-48,50}Th$, and $^{50,52}Cr$ nuclei and the NN realistic interaction Michigan three range Yukawa (M3Y) as a two-body interaction for the CP effect calculations. The probability transition density B (C2) was calculated for some fp-shell nuclei. By use HO potential to calculated form factors and the compared with experimental data for all three maximum momentum transfer areas q when using the Tassie model to include the CP effects, notably at the first and second maximum momentum transfer regions.

Some nuclei in the p- and sd-shells were explored by F. A. Majeed and L. A. Najim (2015)[28], for longitudinal and transverse electron scattering form factors for some positive and negative parity states of ^{7}Li, ^{13}C, and ^{17}O nuclei. The higher energy configurations outside of the p- and sd-shells have been considered in the computation. The microscopic theory has up to four excitation levels, ranging from the basic 1s -1p and 2s -1d orbits up to the upper permissible orbits. It has been shown that the inclusion of higher excited configurations in the calculations of electron scattering form factors and probabilities density is

essential to obtain a reasonable description compared to the available experimental data, which is based on the Cohen-Kurath, Reehal, and Wildenthal interactions, respectively, for the p- and s-shell model space.

A. A. Al-Sammarraie and F. I. Sharrad *et al.* (2015)[29], calculated the electron nucleus scattering form factors for the ^{25}Mg nucleus. The wave functions of radial single-particle matrix elements have been calculated with the Woods-Saxon, harmonic oscillator, and Skyrme (Sk42) potentials. They found that the results of the inelastic transverse form factors agree well with the experimental data when using the Sk42 potential, while the results of the elastic magnetic scattering show a significant difference in the values compared to with experimental data, but the overall shape and other features of the form factors are satisfactory when using the harmonic oscillator potential.

J. Liu *et al.*(2016),[30], researched multiple Coulomb scattering and magnetic scattering of relativistic electrons for ^{27}Al, ^{14}N and ^{39}K nuclei. Nuclear deformation and magnetic moments were taken into account as contributions from the proton hole in the outermost orbit throughout the research. The electron–nucleus scattering was used to obtain the nuclear quadrupole moments Q. The researchers discovered that the results are in good agreement with the experimental quadrupole moments Q by comparing them.

K. S. Jassim and R. A. Abdul-Nabi, (2016)[31], investigated the isoscalar and isovector states of the ^{24}Mg nucleus in sdpf shells were examined for form factors and decreased transition probabilities. The core polarisation effects were computed using Michigan three-range Yakawa as a realistic interaction. The large-scale space computations with core polarisation effects were close to the experimental findings.

On the sdpf-space with Tassie model, K.S.Jassim and S. R. Sahib, (2017)[32], investigated the elastic and inelastic electron scattering, decreased transition probabilities, and the CDD for the ^{19}F nucleus with and without effective charge. The wave function of radial single particle-matrix components was calculated using SKX and HO potentials. The

results were obtained using the shell model code Nushall@MSU. They examined how the result of the CDD and B(WL) calculations is affected by the potential.

J. Liu *et al.* (2017) [33], described the longitudinal form factors for $^{24,25}Mg$, ^{27}Al, ^{31}P, ^{59}Co and ^{23}Na nuclei. The distorted RMF model and the DWBA method were utilised in the calculations. Theoretical longitudinal form factors were quite close to experimental data. The charge distributions of distorted odd-A nuclei were better described by the deformed RMF model.

T. Liang *et al.*(2018)[34], is investigated the elastic electron scattering for $^{126-142}Xe$ nuclei by the deformed scattering model. The researchers found that the minima of the Coulomb form factor of isotopes are directly influenced by the nuclear deformation parameter β_2, not just the charge radius R_C. For the studies of electron scattering, nuclear deformation should be taken into account, especially in high momentum transfers. Nuclear deformation should be taken into account while studying electron scattering, especially when substantial momentum transfer is involved.

K. S. Jassim and S. R. Sahib in (2018)[35] have calculated energy levels for the $^{25-26}Mg$, ^{19}F, and ^{27}Al nuclei by using sdpf-now as effective interaction with the large-scale sdpf model space by using the shell model code. They used the HO and SKX potentials to calculate the wave functions of radial single-particle matrix elements.

The charge density distributions, elastic charge form factors, and size radii for halo ^{11}Be,^{19}C, and ^{11}Li nuclei were computed by A. R. Ridha and Z. M. Abbas in (2018)[36]. Each nucleus core and halo components are separated into two separate sections. The core is examined using HO radial wave functions, whereas the halo is explored using WS potential radial wave functions. For matter density distributions and accessible size radii, there is an excellent match with experimental data.

A. D. Salman *et al.*(2019)[37], calculated the inelastic longitudi-

nal electron scattering form factors for $^{64,66,68}Zn$ nuclei with the HO and WS as a potentials used to calculate the wave functions of radial single-particle matrix elements. To obtain theoretical conclusions, the researchers employed NUSHELL code with M3Y and MSDI as a residual interaction. When compared to experimental data, they discovered that form factors using F5PVH interactions with WS potential are better than those using HO Potential in all regions of momentum transfer.

The coulomb form factors of ^{96}Mg, ^{95}Mg, ^{44}S and, ^{45}S for the oblate and prolate states investigated by J. Liu *et al.*(2019)[38]. The shape configurations of ground states are calculated by relativistic mean field (RMF) model. The researchers discovered that the coulomb form factors of oblate and prolate nuclei are nearly comparable to the shape coexistence of even-even nuclei, but that the calculations for odd-A nuclei diverge noticeably from the coexistence state and prolate or oblate states.

P. Sarriguren et al.(2020)[39], calculated elastic electron scattering within PWBA and within a deformed formalism for odd nuclei of ^{17}O, ^{41}Ca, ^{25}Mg and, ^{59}Co. The researchers compared the theoretical results of both spherical and deformed nuclei with experiment data and they found that the distorted image increases the data's agreement. The odd particle contributes the most to the magnetic form factor in odd-A deformed nuclei, according to the results. In comparison, nucleons play a large role in charge form factors.

The energy levels and transition probabilities B(E2) and B(M1) for $^{21,23}Na$ nuclei were investigated by A. K. Hasan *et al.*(2020)[40]. The calculation performed using USDA and USDB interactions in sd-shell model space. The researchers compared the experimental data to the shell model results and discovered that the empirical data agrees well with theoretical energy level projections.

H. M. Dlshad *et al.*(2020)[41], is investigated inelastic electron-nucleus scattering form factors for ^{9}Be nucleus with CP effects. They used HO potential to calculate single-particle radial wave functions.

They found the ground state Coulomb form factors C0 transitions for M3Y interaction and the ground state charge radii with folding effect best fit the experimental data for Beryllium ^{9}Be nucleus.

Shell model with self-consistent HF computations are used to explore the nuclear structure of the ^{27}Al nucleus. For positive parity states, shell model computations were conducted with the entire sd model space by R.A. Radhi *et al.*(2021)[42], The inferred conclusions for the longitudinal and transverse form factors were reviewed and compared with the available experimental data, according to the researchers. The CP effects have been discovered to be critical in establishing a good description of the data.

I. AH. Ajeel *et al.* (2022)[43], studied the Coulomb C2 and C4 form factors of ^{18}O, ^{20}Ne, and, ^{22}Ne nuclei used the CP calculations, the TM model and the BM collective one were utilized with the Wildenthal (W) and USDA interactions for the sd-shell and used HO, WS and SKX potentials to calculate single-particle radial wave functions. In comparison to model space computations, the inclusion of CP effects good agreement with experimental data. The outcomes of various potentials are compared.

1.3 Aim of the Present Work

The present work aims to study the electron scattering longitudinal form factors for some nuclei as ^{31}P, ^{27}Al, ^{23}Na and many states for ^{25}Mg nucleus by using the shell model in sdpf-space. The calculations have been performed using the large scale model by employing Bohr-Mottelson (BM) collective model. The calculated form factors with sdpfnow as a residual interaction for the studied nuclei will be compared with the available empirical data.

Chapter Two
Shell Model Formalism

2.1 Background for Shell Model

Schrodinger's equation is almost always a part of every quantum mechanical issue. A correct Hamiltonian is one of the most critical phases in this process. When dealing with a multi-body problem like the one in nuclear physics, it is useful, to begin with the assumption of independent particle motion so that the Hamiltonian is written as the sum of individual components from each particle in the nucleus[22],

$$H^{(0)} = \sum_{i=1}^{A} [T_i + U(r_i)] \tag{2.1}$$

Where $H^{(0)}$ is the unperturbed Hamiltonian, T_i and $U(r_i)$ are the Kinetic energy and the potential energy, respectively.Since the Pauli Exclusion Principle mandates that the wave functions for identical particles be anti-symmetric, the eigenfunctions to the above equation are given by the Slater determinant, which, for a two-particle system, is written as[22],

$$\phi_{\alpha_1\alpha_2} = \frac{1}{\sqrt{2!}} \begin{vmatrix} \varphi_{\alpha_1}(1) & \varphi_{\alpha_1}(2) \\ \varphi_{\alpha_2}(1) & \varphi_{\alpha_2}(2) \end{vmatrix} = \frac{1}{\sqrt{2!}} [\varphi_{\alpha_1}(1)\varphi_{\alpha_2}(2) - \varphi_{\alpha_1}(2)\varphi_{\alpha_2}(1)] \tag{2.2}$$

Where φ_{α_1},φ_{α_2} are the single-particle wave-functions, given the product of radial and angular components. The only part of this expression that is not explicitly defined is the radial part, $R_{nl}(r)$. The details of this function depend on the form of the potential $U(r)$ of the eq. (3.1). It turns out that the choice of this potential is not straight forward.
The shell model assumes that the interaction between nucleons in the an average central potential can approximate the nucleus, called the mean-field potential. The radial components of the single-nucleon wave functions used in this work are obtained from three different potentials, the harmonic oscillator (HO) potential with size parameter b, Woods-Saxon (WS), and Skyrme (SKX) potential. For Skyrme interaction, it can be expressed as effective two-body potential.

2.1.1 Harmonic Oscillator (HO) Potential

Three-dimensional oscillator potential is a suitable approximation for nuclear potential with light nuclei because it can readily manipulate the wave functions of single particles. From the mean-field approximation, each nucleon of mass (m) moves independently in a potential that represents the average interaction with the other nucleons in a nucleus. Supposing that the potential depth at the center of the nucleus is U_o, then for each particle moves in a spherically symmetric harmonic oscillator potential with angular frequency (ω), the Hamiltonian becomes[44]:

$$H_o = \frac{-h^2}{2m}\nabla^2 + \frac{m\omega^2 r^2}{2} - U_o \tag{2.3}$$

Where $U_o = \frac{m\omega^2 R^2}{2}$ and $R = R_0 A^{1/3}\ fm$.
The eigenvalue (Schrodinger's) equation for the wave function $\langle r, \theta, \varphi | nlm_l \rangle$ is given by[45]:

$$H_o|nlm_l\rangle = \epsilon_{nl}|nlm_l\rangle = \epsilon_{nl}|nl\rangle|lm_l\rangle \tag{2.4}$$

Where n, l and m_l are the principal, orbital, and magnetic quantum numbers, respectively. The corresponding wave functions are represented by:

$$\begin{aligned} &\langle r, \theta, \varphi | nlm_l \rangle = R_{nl}(r) Y_{lm_l}(\theta, \varphi) \\ &\langle r | nl \rangle = R_{nl}(r) \\ &\langle \theta, \varphi | lm_l \rangle = Y_{lm_l}(\theta, \varphi) \end{aligned} \tag{2.5}$$

Where $Y_{lm_l}(\theta, \varphi)$ and $R_{nl}(r)$ are the spherical harmonics and the radial wave functions, respectively. The radial wave function for the HO potential is given by[22]:

$$\begin{aligned} R_{nl}(r) = &\sqrt{\frac{2^{l-n+3}(2l+2n-1)!!}{[(2l+1)!!]^2 (n-1)!\ b^3\ \sqrt{\pi}}}\ e^{-r^2/2b^2} \\ &\sum_{k=0}^{n-1} \frac{(-1)^k\ 2^k\ (2l+1)!!}{(n-k-1)!\ k!\ (2l+2k+1)!!} (r/b)^{2k+1} \end{aligned} \tag{2.6}$$

The HO size parameter b which relates to the mass of nucleon (m) and frequency (ω) as associated with the HO potential[46]

$$b = \sqrt{\frac{h/2\pi}{m\omega}} \tag{2.7}$$

One can reproduce the magic numbers by adding the strong spin-orbit interaction term V_{ls} to the single-particle Hamiltonian[22]

$$V_{ls} = f(r)\vec{l}.\vec{s} \tag{2.8}$$

Where $f(r)$ is a radial function, the single-particle Hamiltonian becomes:

$$H_o = \frac{-h^2}{2m}\nabla^2 + \frac{m\omega^2 r^2}{2} - U_o + f(r)\vec{l}.\vec{s} \tag{2.9}$$

For the jj coupling scheme between the spinor state function $|Sm_s\rangle$ and the angular part of the spatial state function $|lm_l\rangle$[47]:

$$|nljm_j\rangle = \sum_{m_l m_s} |Sm_s\rangle|nlm_l\rangle\langle lm_l Sm_s|nljm_j\rangle \tag{2.10}$$

Therefore, the Single-Particle Energy (SPE) is a function of the total nucleon quantum number (j) and the $\vec{l}.\vec{s}$ potential causes a separation of the (j=l+1/2) or (j=l-1/2) levels:

$$\langle nljm_j|V_{ls}|nljm_j\rangle = \langle f(r)\rangle_{nl} \begin{cases} -(l+1)/2 & for\ j = l - 1/2 \\ l/2 & for\ j = l + 1/2 \end{cases} \tag{2.11}$$

For the HO potential, the value of $\langle f(r)\rangle_{nl}$, depends on the mass number of the nucleus that is evaluated from [48] and $\langle f(r)\rangle_{nl}$ given by:

$$\langle f(r)\rangle_{nl} = \langle nl|f(r)|nl\rangle \approx -20A^{-2/3}\ Mev \tag{2.12}$$

The Pauli exclusion principle allows for a minimum number of oscillator quanta N to be included in a shell model configuration, and are then referred to as N$\hbar\omega$ configurations. It is found advantageous to treat proton and neutron (neglecting the difference in masses) as two charge states of one particle, called the nucleon. To distinguish the two charge states of the nucleon, the isospin quantum number has been included in analogy with the spin quantum number, t =1/2 with two possible projections $t = \pm 1/2$.Hence, the state of each nucleon defined by the quantum numbers n, l, j, m_l, t [49].

2.1.2 Woods-Saxon Potential (WS)

In terms of the one-body potential, the WS potential is an excellent option. In order to calculate the total binding energy, WS (or any other one-body potential) cannot be utilized since it does not account for unique two-body interactions[46]. To get the best match for nuclear single-particle energies and nuclear radii, we use the WS parameters. Solving the equation yields the radial components of the single-nucleon wave functions of the WS potential[50].

$$[-\frac{\hbar^2}{2\mu}\frac{d^2}{dr^2} + \frac{\hbar^2\, l(l+1)}{2\mu r^2} + U(r)]R(j,r) = \epsilon R(j,r) \tag{2.13}$$

Where $\mu = m(p/n)(A-1)/A$ is the reduced mass. The potential $U(r)$ include central, spin-orbital and coulomb parts and given by[51]:

$$U(r) = V_o(r) + V_{ls}(r)l.s + \delta_{pn}V^c(r) \tag{2.14}$$

where V_o is the nuclear potential depth, δ_{pn} is the equal to 1 for protons and 0 for neutrons, $V_o(r)$ is the spin-independent central potential, $V^c(r)$ is the Coulomb potential. The central Woods-Saxon potential is:

$$V_o(r) = V_o[1 + exp(r - R_o)/a_o]^{-1} \tag{2.15}$$

The Coulomb potential for protons are based upon the Coulomb potential for a sphere of radius R_c given by [49]:

$$V^c(r) = \begin{cases} \frac{ze^2}{2R_c}[3 - (r/R_c)^2], & r \le R_c \\ \frac{ze^2}{r}, & r \ge R_c \end{cases} \tag{2.16}$$

The spin-orbit potential $V_{ls}(r)$ is based [49] on the usual derivative of a Fermi shape:

$$V_{ls}(r) = V_{ls}\frac{1}{r}\frac{d}{dr}[1 + exp(r + R_{ls}/a_{ls})]^{-1} \tag{2.17}$$

Where R and a are the nuclear radius, and the surface diffuseness, respectively. The radii R_o, R_{ls}, and R_c are usually expressed as:

$$R_i = r_i A^{1/3}, \quad i = 0, ls\ or\ C \tag{2.18}$$

A typical set of parameters for the WS potential are $V_o = -53Mev$, $V_{ls} = 22Mev$, $r_o = r_{ls} = 1.25fm$, $r_c = 1.20fm$ and $a_o = a_{ls} = 0.65fm$.One can find in the literature many other sets of parameters which are better for specific nuclei or mass regions[49].

2.1.3 Skyrme Interaction (SK)

In 1958, Skyrme created the Skyrme interaction[52], which can be expressed as the sum of two- and three-body parts[53]. The SK forces with the three-body term replaced by a density-dependent two-body term. The SK force can be decomposed into a central V^c, spin-orbit V_{ls} and tensor contribution V^t. V^t is usually neglected[54]. The two body term of SK force is written as a short range expansion in the form[55]

$$V^{SK} = V^c + V_{ls} + V^t \tag{2.19}$$

$$\begin{aligned} V^{SK} =& t_o(1+\chi_o\hat{p}_\sigma)\delta(\vec{r}) + \frac{1}{2}t_1(1+\chi_1\hat{p}_\sigma)(\hat{k'}^2\delta(\vec{r}) + \delta(\vec{r})\hat{k}^2) + t_2(1+\chi_2\hat{p}_\sigma) \\ & \hat{k'}\delta(\vec{r})\vec{k} + \frac{1}{6}t_3(1+\chi_3\hat{p}_\sigma)\rho^\alpha(R)\delta(\vec{r}) + it_4\hat{k'}\delta(\vec{r})(\vec{\sigma}_i + \vec{\sigma}_j) \end{aligned} \tag{2.20}$$

Where $\vec{k} = (\nabla_1 - \nabla_2)/2i$ and $\vec{k'} = (\nabla'_1 - \nabla'_2)/2i$ are relative momentum operators. $\delta(\vec{r})$ is the delta function. $\hat{p}_\sigma$ is the spin-exchange operator, σ the vector of Pauli spin matrices, and the SKyrme force parameters are $t_o, t_1, t_2, t_3, t_4, \chi_o, \chi_1, \chi_2, \chi_3$.

2.2 Bohr-Mottelson (BM) Collective Model

It has been shown that the shell model can describe many aspects of the nucleus's ground state and some stimulated states. However, it fails conspicuously in explaining the observed significant electric quadrupole moments (Q) of the nuclei in many cases and the quadrupole transition rates B(E2). J. Rainwater(1950)[56] was the first who tried to explain these failures of the shall model by introducing the idea of deformation in the shape of the nuclear core due to the motion of the odd loose nucleon outside the core in odd A nuclei. The motion leads to a polarization of the even-even core, thus assuming a spheroidal shape. Such

deformation would cause the quadrupole moment to be higher than the single-particle value. A. Bohr and B. Mottelson (1953) further elaborated the model, combining the single-particle and collective motions into a unified model, which gave a complete description of the deformed nuclei[57].

Bohr and Mottelson proposed the 5D quadrupole collective Hamiltonian, which describes the quadrupole vibrations and rotation in a unified manner. It is written as[[58],[59]]:

$$H_{coll} = T_{vib} + T_{rot} + V(\beta, \gamma) \tag{2.21}$$

$$T_{vib} = \frac{1}{2} D_{\beta,\beta}(\beta,\gamma)\dot{\beta}^2 + D_{\beta,\gamma}(\beta,\gamma)\dot{\beta}\dot{\gamma} + \frac{1}{2} D_{\gamma,\gamma}(\beta,\gamma)\dot{\gamma}^2 \tag{2.22}$$

$$T_{rot} = \frac{1}{2} \sum_{k=1}^{3} J_k(\beta,\gamma)\dot{\varphi}_k^2 \tag{2.23}$$

Where $\dot{\varphi_k}$ are the components of the rotational angle on the three intrinsic axes. The quadrupole deformation (β, γ) and the rotation angles φ_k are treated as dynamical variables, and $(\dot{\beta}, \dot{\gamma})$ represent their time-derivatives. The φ_k is called angular velocities. The quantities $(D_{\beta,\beta}, D_{\beta,\gamma}, and D_{\gamma,\gamma})$ represent inertial masses of the vibrational motion and T_{vib} represent the kinetic energies of vibrational motion.

The quantities $J_k(\beta, \gamma)$ in the rotational energy T_{rot} represent the moments of inertia with respect to the intrinsic (body-fixed) axes. This body-fixed frame, coupled with a time-dependent mean-field in real-time, can serve as a reference for defining the intrinsic axes.The term $V(\beta, \gamma)$ represent the potential energy as a function of β and γ.
The equation of the Bohr-Mottelson collective Hamiltonian from eq.(2.21) is often referred to as the liquid drop model.However, what should emphasize is that the analogy with the classical liquid drop is irrelevant to low-frequency quadrupole collective motions. Already in 1950's, it was recognized that the nucleus is "an unusual idealized quantum fluid and one is dealing with a most interesting new form of matter"[60].
Most nuclei may be regarded as a super-fluid of tiny size with a radius of a few femtometers, and the nature of nuclear deformation is essentially

different from that of surface shape oscillations of the classical liquid drop; that is, the nuclear deformation is associated with quantum shell structure and spontaneous breaking of the spherical symmetry in the self-consistent mean filed.

The form of collective Hamiltonian from eq.(2.21) is quite general and applicable to the various finite many-body systems, but values reveal the specific dynamical properties of the system of interest and the (β, γ) dependence of the collective inertia masses $(D_{\beta\beta}, D_{\beta\gamma}, D_{\gamma\gamma}, J_k)$ as well as the potential energy $V(\beta, \gamma)$.It is thus essential to extract these variables microscopically and compare them with what experimental data reveal to comprehend the dynamic features of the nucleus.
The Hamiltonian from eq.(2.21) is given in terms of the five curvilinear coordinates (β, γ and the three Euler angles which are connected with φ by a linear transformation) and their time derivatives. For quantization in curvilinear coordinates, we can adopt the so-called Pauli prescription[61].The microscopic derivation of the Bohr-Mottelson collective Hamiltonian. The quantized 5D quadrupole collective Hamiltonian takes the following form[59]:

$$\hat{H}_{coll} = \hat{T}_{vib} + \hat{T}_{rot} + V(\beta, \gamma) \tag{2.24}$$

Here, the vibrational Kinetic energy term $\hat{T}_{vib}$ is given by:

$$\begin{aligned}\hat{T}_{vib} = &-\frac{1}{2\sqrt{WR}}\{\frac{1}{\beta^4}[\frac{\partial}{\partial\beta}(\beta^2\sqrt{\frac{R}{W}}D_{\gamma\gamma}\frac{\partial}{\partial\beta}) - \frac{\partial}{\partial\beta}(\beta^2\frac{R}{W}D_{\beta\gamma}\frac{\partial}{\partial\gamma}] \\ &+ \frac{1}{\beta^2\sin(3\gamma)}(-\frac{\partial}{\partial\gamma}(\sqrt{\frac{R}{W}}\sin(3\gamma)D_{\beta\gamma}\frac{\partial}{\partial\beta})) \\ &+ \frac{\partial}{\partial\gamma}(\sqrt{\frac{R}{W}}\sin(3\gamma)D_{\beta\beta}\frac{\partial}{\partial\beta})\}\end{aligned} \tag{2.25}$$

Where the rotation energy term $\hat{T}_{rot}$ is given by:

$$\hat{T}_{rot} = \sum_{k=1}^{3}\frac{\hat{I}_k^2}{2J_K(\beta, \gamma)} \tag{2.26}$$

With $\hat{I}_k^2$ denoting three components of the angular-momentum operator with respect to the intrinsic axis. In this study, we use the unit with

$\hbar = 1$.
In the above equation[62]:

$$\beta^2 W(\beta,\gamma) = D_{\beta\beta}(\beta,\gamma)D_{\gamma\gamma}(\beta,\gamma) - D^2_{\beta\gamma}(\beta,\gamma) \tag{2.27}$$

$$R(\beta,\gamma) = D_1(\beta,\gamma)D_2(\beta,\gamma)D_3(\beta,\gamma) \tag{2.28}$$

and $D_k(\beta,\gamma)$ $(k = 1,2,3)$ are the rotational inertial functions related to the moments of inertia by[59]:

$$J_k(\beta,\gamma) = 4\beta^2 D_k(\beta,\gamma)\sin^2(\gamma - 2\pi k/3) \tag{2.29}$$

If all inertial masses $(D_{\beta\beta}, D_{\gamma\gamma}\beta^{-2}, D_1, D_2, D_3)$ are replaced by a common constant:
D and $D_{\beta\gamma}$ is ignored, the above $\hat{T}_{vib}$ is reduced to:

$$\hat{T}_{vib} = -\frac{1}{2D}\left(\frac{1}{\beta^4}\frac{\partial}{\partial\beta}\beta^4\frac{\partial}{\partial\beta} + \frac{1}{\beta^2\sin(3\gamma)}\frac{\partial}{\partial\gamma}\sin(3\gamma)\frac{\partial}{\partial\gamma}\right) \tag{2.30}$$

Only small-amplitude vibrations around a spherical Hartree-Fock Bogoliubov (HFB) equilibrium may be valid for such a drastic approximation in this context. The need to go beyond this simplest approximation for the inertia masses has been pointed out[57].For recent experimental data and phenomenological analyses of this problem[61].
The collective Schrodinger equation is[62][57]:

$$\left(\hat{T}_{vib} + \hat{T}_{rot} + V(\beta,\gamma)\right)\psi_{\alpha IM}(\beta,\gamma,\Omega) = E_{\alpha I}\,\psi_{\alpha IM}(\beta,\gamma,\Omega) \tag{2.31}$$

The collective wave function in the laboratory frame, $\psi_{\alpha IM}(\beta,\gamma,\Omega)$ is the function of β,γ and Ω set of three Euler angles Ω. It is specified by the total angular momentum I, its projection onto the z-axis in the laboratory frame M, and α the distinguishes the eigenstates possessing the same value of I and M. With the rotational wave function D^I_{MK}, they are written as[59]:

$$\psi_{\alpha IM}(\beta,\gamma,\Omega) = \sum_{k=even}\phi_{\alpha Ik}(\beta,\gamma)\langle\Omega|IMK\rangle \tag{2.32}$$

Where

$$\langle\Omega|IMK\rangle = \sqrt{\frac{2I+1}{161\pi^2(1+\delta_{k_0}}}[D^I_{MK}(\Omega) + (-1)^I D^I_{M,-k}(\Omega)] \tag{2.33}$$

The vibration wave functions in the body-fixed frame,$\phi_{\alpha IK}(\beta,\gamma)$, are normalized as:

$$\int d\beta\, d\gamma\, \sqrt{G(\beta,\gamma)}\, |\phi_{\alpha I}(\beta,\gamma)|^2 = 1 \tag{2.34}$$

Where

$$|\phi_{\alpha I}(\beta,\gamma)|^2 = \sum_{k=even} |\phi_{\alpha Ik}(\beta,\gamma)|^2 \tag{2.35}$$

and the volume element is given by $\sqrt{G(\beta,\gamma)}\, d\beta\, d\gamma$ with:

$$G(\beta,\gamma) = 4\beta^8 W(\beta,\gamma) R(\beta,\gamma) \sin^2(3\gamma) \tag{2.36}$$

Thorough discussions of symmetries of the collective wave functions and the boundary condition for solving the collective Schrodinger equation are given in Refs.[63][64]]
Inserting (2.32) into the collective Schrodinger equation (2.31), we obtain the egenvalue equation for vibrational wave functions[65].

$$\begin{aligned}[\hat{T}_{vib} + V(\beta,\gamma)]\phi_{\alpha IK}(\beta,\gamma) + \sum_{k'=even} \langle IMK|\hat{T}_{rot}|IMK'\rangle \phi_{\alpha IK'}(\beta,\gamma) \\ = E_{\alpha I}\ \phi_{\alpha IK}(\beta,\gamma)\end{aligned} \tag{2.37}$$

Solving this equation, we obtain quantum spectra and collective wave functions.

Chapter Three
General Theory

3.1 Electron Scattering

Plane waves are used to represent electrons in the electron scattering theory. In a non-relativistic situation, the Schrodinger equation is satisfied by propagating a free electron in space:

$$-\frac{\hbar^2}{2m_o}\nabla^2\psi = -i\hbar\frac{\partial\psi}{\partial t} \tag{3.1}$$

For an infinity large free space, the plane wave solution of the equation (3.1) written as:

$$\psi = exp(2\pi i k_o.r + i\omega' t) \tag{3.2}$$

Where $k_o = 1/\lambda$ is the electron wave number and ω' is angular frequency.
The plan-wave Born approximation's (PWBA) differential scattering cross-section for scattering an electron into a material at an angle $d\Omega$ from a charged nucleus Ze with mass M is given by[66][67][68]:

$$\frac{d\sigma}{d\Omega} = \sigma_M \; f_{rec} \; \sum_J |F_J(q,\theta)|^2 \tag{3.3}$$

Where $F_J(q,\theta)$ is scattering amplitude and σ_M is the Mott cross-section for scattering from a point like nuclear charge Ze and is defined as[69]:

$$\sigma_M = [\frac{Z\alpha\cos(\theta/2)}{2E_i sin^2(\theta/2)}]^2 \tag{3.4}$$

Where θ is the angle of scattering, $\alpha = e^2/hc = 1/137$ is the fine structure constant, Z is the atomic number of the target nucleus and E_i is the energy of incident electron. The recoil factor of the nucleus is given by[66]:

$$f_{rec} = [1 + \frac{2E_i}{M} sin^2(\theta/2)]^{-1} \tag{3.5}$$

The energy transfer is $\omega = E_i - E'$, E_i is the incident electron energy, E' is the scattering electron energy, the three momentum transfer is q and the four-momentum transfer is q_μ is given by[66]:

$$q_\mu^2 = q^2 - \omega^2 = 4EE' sin^2(\theta/2) \tag{3.6}$$

The form factor is given by the well-known multi-pole as a function of momentum transfer q [70]:

$$|F_J^{\eta}(q)|^2 = \frac{4\pi}{Z^2(2J_i+1)}|\langle J_f\|\hat{T}_J^{\eta}(q)\|J_i\rangle|^2 \tag{3.7}$$

Transverse (T) and longitudinal (L) are denoted by the superscript η in the electron scattering multi-pole operator $T_J^{\eta}(q)$, J_i and J_f are the total angular momentum of the initial and final states, respectively. When using the theory of Wigner-Eckert in isospin space, the form factor can be written in terms of matrix element reduced contain both the angular momentum (J) and isospin (T) and is given as:

$$\begin{aligned}|F_J^{\eta}(q)|^2 =& \frac{4\pi}{Z^2(2J_i+1)}|\sum_{T=0,1}(-1)^{T_f-T_{zf}}\begin{pmatrix} T_f & T & T_i \\ -T_{Zf} & M_T & T_{Zi}\end{pmatrix} \\ & \langle J_f T_f|||\hat{T}_{JT}^{\eta}(q)|||J_i T_i\rangle|^2\end{aligned} \tag{3.8}$$

Where $T_Z = |\frac{Z-N}{2}|$
The rule of angular momentum and isospin can be written as:

$$|J_i - J_f| \leq J \leq J_i + J_f \tag{3.9}$$

$$|T_i - T_f| \leq T \leq T_i + T_f \tag{3.10}$$

3.2 The One Body Density Matrix Elements (OBDM)

The work of Lee and Kurath is where the OBDM components are found. The OBDM elements used in this work is related to the transition amplitudes.$A_{J,t_z}(j_a, j_b)$ by:[71]

$$OBDM^{J,t_z}(i,f,j_a,j_b) = \sqrt{2J_f+1}\frac{A_{J,t_z}(j_a,j_b)}{\sqrt{2J+1}} \tag{3.11}$$

The transformation from L-S coupling basis to J-J coupling is given by[71]:

$$A_{J,t_z}(j_a,j_b) = \sum_{LS}(\hat{j_a}\hat{j_b}\hat{L}\hat{S})^{1/2}\begin{Bmatrix} l_b & 1/2 & j_b \\ l_a & 1/2 & j_a \\ L & S & J\end{Bmatrix} A_{J,t_z}(LS) \tag{3.12}$$

Where the bracket $\left\{ \begin{array}{c} .... \\ .... \\ .... \end{array} \right\}$ is the 9j-symbols and $\hat{J} = 2J+1$. In isospin representation, the value of the $OBDM^{J,T}$ is obtained from the value of $OBDM^{J,t_z}$ as[72]:

$$OBDM^{J,t_z} = (-1)^{T_f - T_z}\{\sqrt{2}\begin{pmatrix} T_f & 0 & T_i \\ -T_Z & 0 & T_Z \end{pmatrix}\frac{OBDM(\Delta T = 0)}{2} + 2t_z\sqrt{6} \begin{pmatrix} T_f & 0 & T_i \\ -T_Z & 0 & T_Z \end{pmatrix}\frac{OBDM(\Delta T = 1)}{2}\} \tag{3.13}$$

With $t_z = 1/2$ for a proton and -1/2 for a neutron. The bracket $\begin{pmatrix} .... \\ .... \end{pmatrix}$ is 3j-symbol.

3.3 The Reduced Single-Particle Matrix Elements

The sum of the product of the elements of the One Body Density Matrix (OBDM) times the single particle-matrix elements is the reduced matrix element of the required operator T^{η}_{Λ} and given as[73]:

$$\langle J_f \| \hat{T}^{\eta}_{J,t_Z} \| J_i \rangle = \sum_{a,b} OBDM^{J,t_Z}(J_i, J_f, a, b) \langle a \| \hat{T}^{\eta}_{J,t_Z} \| b \rangle \tag{3.14}$$

Where $t_z = -1/2$ for neutron and $1/2$ for proton. J is the multi-polarity and J_i and J_i are initial and final states of nucleus,respectively.
$|a\rangle$ and $|b\rangle$ are the single-particle wave function for initial and final states [73]:

$$|a\rangle = |n_a l_a\rangle |j_a m_a\rangle |t t_z\rangle \tag{3.15}$$

$$|b\rangle = |n_b l_b\rangle |j_b m_b\rangle |t t_z\rangle \tag{3.16}$$

Everyplace (n_a,n_b) is the principle quantum numbers, (l_a, l_b) is the orbital angular momentum numbers, (j_a,j_b) is the total single-particle angular momentum quantum numbers, (m_a,m_b) is projection of (j_a,j_b), respectively and $|tt_z\rangle$ is the single-particle isospin state.

3.4 The Longitudinal Operator's Reduced Single-Particle Matrix Elements

The nucleon in a well-defined shell model state interacts with the electron in the single-particle model. It is the interaction of electrons with the nucleus's charge distribution that generates the longitudinal scattering, as described by the Coulomb form factors. The longitudinal operator, which is an irreducible operator of rank J in the nuclear Hilbert space, is defined as[66]:

$$\hat{T}^{L}_{J,M}(q,t_z) = \int d\vec{r}\; j_J(qr)\; Y_{JM}(r)\; \hat{\rho}(\vec{r},t_z) \tag{3.17}$$

Where $j_J(qr)$ is the spherical Bessal function, $Y_{JM}(r)$ is the spherical harmonic and $\hat{\rho}(\vec{r},t_z)$ is the single nucleon charge density operator is given by[74]:

$$\hat{\rho}(\vec{r},t_z) = e(t_z)\delta(\vec{r}-\vec{r_i}) \tag{3.18}$$

Where $\delta(\vec{r}-\vec{r_i})$ is Dirac deita function and $e(t_z) = \frac{1+2t_z}{2}$. From the equations (2.17) and (2.18), one obtains:

$$\hat{T}_{J,M}(q,t_z) = e(t_z)\; j_J(qr)\; Y_{JM}(r) \tag{3.19}$$

The longitudinal operator of the reduced single-particle matrix element between the initial $|n_b,l_b,j_b\rangle$ and final $|n_a,l_a,j_a\rangle$ states can be given as[66]:

$$\begin{aligned}\langle n_a,l_a,j_a\|\hat{T}_{J,t_z}\|n_a,l_a,j_a\rangle =& e(t_z)\langle n_a,l_a|j_J(qr)|n_a,l_a\rangle \\ & \langle l_a 1/2\; j_a\|Y_J(r)\|l_b 1/2\; j_b\rangle\end{aligned} \tag{3.20}$$

Spherical harmonics are characterized by a decreased matrix element given by[67]:

$$\begin{aligned}\langle l_a 1/2\; j_a\|Y_J(r)\|l_b 1/2\; j_b\rangle =& 1/2(-1)^{j_a+1/2}[1+(-1)^{l_a+l_b+J}] \\ & \sqrt{\frac{(2j_a+1)(2j_b+1)(2J+1)}{4\pi}} \begin{bmatrix} j_a & J & j_b \\ 1/2 & 0 & -1/2 \end{bmatrix}\end{aligned} \tag{3.21}$$

The single-particle matrix element of the Bessel's function in spherical coordinate is[75]:

$$\langle n_a l_a | j_J(qr) | n_b l_b \rangle = \int_0^\infty dr r^2 j_J(qr) R_{n_a,l_a}(r) R_{n_b,l_b}(r) \tag{3.22}$$

Where $R_{n_a,l_a}(r)$ and $R_{n_b,l_b}(r)$ are the radial parts of the single-particle wave function for final and initial states. A Harmonic Oscillator (HO) with size parameter b and the radial wave function component is used to solve Schrodinger's equation. The radial matrix elements of Bessel function can be solved analytically as[73]:

$$\begin{aligned}\langle n_a l_a | j_J(qr) | n_b l_b \rangle =& \frac{2^J}{(2J+1)!!} Y^{J/2} exp(-Y)[(n_b-1)!(n_a-1)!]^{1/2} \\ & [\Gamma(n_b+l_b+1/2)\Gamma(n_a+l_a+1/2)]^{1/2} \sum_{m_b=0}^{n_b-1} \sum_{m_a=0}^{n_a-1} \\ & \frac{(-1)(m_b+m_a)}{m_a! m_b!} \frac{1}{(n_{b-m_b}-1)!(n_a-m_a-1)!} \\ & \frac{\Gamma(1/2(l_b+la+2m_b+2m_a+J+3)}{\Gamma(m_b+l_b+3/2)\Gamma(m_a+l_a+3/2)} \\ & F(1/2(J-l_a-l_a-2m_b-2m_a); J+3/2; Y)\end{aligned} \tag{3.23}$$

Where $Y = (bq/2)^2$, Γ is gamma function and F is the confluent hypergeometric function, which may be evaluated by using[73]:

$$F(a;b;y) = 1 + \frac{a}{b}y + \frac{a(a+1)}{b(b+1)}\frac{y^2}{2!} + ... \tag{3.24}$$

It is possible to express the longitudinal form factor in terms of the reduced many-particles matrix element of the transition operator as[22]:

$$|F^L_{J,t_z}(q)|^2 = \frac{1}{z^2}\frac{4\pi}{2J_i+1}\langle J_f \| \hat{T}^L_{Jt_z} \| J_i \rangle \tag{3.25}$$

The reduced many-partical matrix element with spin-space is given by[73]:

$$\langle J_f \| \hat{T}^L_{Jt_z} \| J_i \rangle = \sum_{a,b} OBDM(J_f, J_i, a, b, J, t_z) \langle a \| \hat{T}^L_{Jt_z} \| b \rangle \tag{3.26}$$

And can be written as[73]:

$$\langle J_f \| \hat{T}^L_{Jt_z} \| J_i \rangle = e(t_z) \int_0^\infty dr r^2 j_J(qr) \rho_{Jt_z}(i,f,r) \tag{3.27}$$

Where ρ_{Jt_z} is the transition charge density and given by[73]:

$$\rho_{Jt_z}(r) = \sum_{a,b} OBDM^{Jt_z}(i,f,a,b) \langle n_a l_a j_a \| Y_J \| n_b l_b j_b \rangle R_{n_a l_a}(r) R_{n_b l_b}(r) \tag{3.28}$$

Practical experiences showed that the electron is not a point but has a finite size that must be corrected for. So the equation of nuclear form factor must be multiplied by this correction which is found to be as[76]:

$$F_{f.s}(q) = e^{\frac{-0.43q^2}{4}} \tag{3.29}$$

And the center of mass correction is given by[76]:

$$F_{c.m}(q) = e^{\frac{q^2 b^2}{4A}} \tag{3.30}$$

Where A is the nuclear mass number and b is the Harmonic-Oscillator size parameter. Corrections to eliminate the spurious states that arise when using a shell model wave function are applied to the center of mass. The effects of limited nucleus size, center of mass motion, and Coulomb distortion of electron waves must be taken into consideration when calculating the form factor.Thus, given multi-polarity J's form factor in terms of the matrix elements reduced both in angular momentum and isospin spaces and using Wigner-Eckart theory as[77]:

$$\begin{aligned} |F^\eta_J(q)|^2 =& \frac{4\pi}{Z^2(2J_i+1)} | \sum_{T=0,1} (-1)^{T_f - T_z f} \begin{pmatrix} T_f & T & T_i \\ -T_{Zf} & M_T & T_{Zi} \end{pmatrix} \\ & \langle \Gamma_f \| | \hat{T}^\eta_{J,T}(q) | \| \Gamma_i \rangle | F_{f.s}(q) |^2 | F_{c.m}(q) |^2 \end{aligned} \tag{3.31}$$

Where $T_z = \frac{Z-N}{2}$. For electron scattering $T_{zi} = T_{zf}$ and $M_T = 0$ The plane wave Born approximation is used to formulate the form factors presented thus far.

The single-particle energies are given by[22]:

$$e_{nlj} = (2n + l - 1/2)\hbar\omega + \begin{cases} -1/2(l+1)\langle f(r) \rangle_{nl} & for\ j = l - 1/2 \\ 1/2l \langle f(r) \rangle_{nl} & for\ j = l + 1/2 \end{cases} \tag{3.32}$$

With

$$\begin{aligned} \langle f(r)\rangle_{nl} \approx & 20A^{-2/3}Mev, \\ & \hbar\omega = 45A^{-1/3} - 25A^{-2/3} \end{aligned} \tag{3.33}$$

The momentum transfer is enhanced to first order by electron Coulomb distortions, resulting in an effective transfer q_{eff} which is given by[78] [79]:

$$q_{eff} = q[1 + \frac{3}{2}\frac{Ze^2}{ER_c}] \tag{3.34}$$

Where $R_c = \sqrt{\frac{5}{3}}R_{rms}$ is the root mean square (rms) charge radius.

3.5 The Longitudinal Form Factor

It is at the photon point that we determine the electromagnetic transition probability, where the momentum transfer $q = k = E_x/\hbar c$, where E_x is the excitation energy.The form factor at (q=k) is[77]:

$$|F_J^L(k)|^2 = \frac{4\pi}{(2J_i+1)Z^2} \mid \int_0^\infty dr\, r^2 j_J(kr)\rho_J(i,f,r)|^2 \tag{3.35}$$

For this value of q, the center of mass and finite nucleon size correction factors are almost equal to one.
At $q = k = E_x/\hbar c$

$$j_J(kr) = \frac{(kr)^J}{(2J+1)!!}(1 - \frac{1}{2}\frac{(kr)^J}{(2J+3)} + ...) \tag{3.36}$$

Retaining only the leading term in the series expansion of $j_J(kr)$, one obtains:

$$j_J(kr) \approx \frac{(kr)^J}{(2J+1)!!} \tag{3.37}$$

Then equation (3.35) becomes:

$$|F_J^L(k)|^2 = \frac{4\pi}{(2J_i+1)Z^2}\ [\frac{(k)^J}{(2J+1)!!}]^2 \mid \int_0^\infty dr\, r^{J+2}\rho_J(i,f,r)|^2 \tag{3.38}$$

In the PWBA, the longitudinal form factor is given by Fourier transformation of the transition density $\rho_{fi}(r)$[66]:

$$|F_c(q)|^2 = \frac{1}{Z^2} \sum_{M_i,M_f} |\rho(q)|^2 \tag{3.39}$$

Where

$$\rho(q) = \int e^{iq.r} \langle J_f M_f | \hat{\rho}(r) | J_i M_i \rangle \tag{3.40}$$

The one-body density operator $\hat{\rho}^{(1)}(\vec{r})$ may be used to represent the density distribution of an A-point nucleon system and given by means of the Dirac delta function as[80]:

$$\hat{\rho}^{(1)}(\vec{r}) = \sum_{i=1}^{A} \delta(\vec{r} - \vec{r}_i) e_i \tag{3.41}$$

For the one-body density operator, the many-particle wave function ψ may be used to express the expected value and written as[70]:

$$\begin{aligned}\langle \psi(\vec{r}_1, \vec{r}_2, ...\vec{r}_A) | \hat{\rho}^{(1)}(\vec{r}) | \psi(\vec{r}_1, \vec{r}_2, ...\vec{r}_A) \rangle = & \sum_{i=1}^{A} \int_0^{\infty} \psi^*(\vec{r}_1, \vec{r}_2, ...\vec{r}_A) \delta(\vec{r} - \vec{r}_i) \\ & \psi(\vec{r}_1, \vec{r}_2, ...\vec{r}_A) d\vec{r}_1 d\vec{r}_2 ... d\vec{r}_A\end{aligned} \tag{3.42}$$

The single-particle wave function $\phi_i(\vec{r}_j)$ may be used to represent the nuclear many-particle wave function ψ in terms of Slater determinants and given by[70]:

$$\psi(\vec{r}_1, \vec{r}_2, ...\vec{r}_A) = \frac{1}{\sqrt{A!}} det \phi_i(\vec{r}_j) \tag{3.43}$$

Then, the coordinates are integrated to get the final result[70]

$$\rho_o(r) = \langle \psi(\vec{r}_1, \vec{r}_2, ...\vec{r}_A) | \hat{\rho}^{(1)}(\vec{r}) | \psi(\vec{r}_1, \vec{r}_2, ...\vec{r}_A) \rangle \tag{3.44}$$

Therefore, the density distribution of a system containing A nucleons may be obtained in terms of the single-particle wave function as[81]:

$$\rho_o(r) = \sum_{i=1}^{A} |\phi_i(\vec{r})|^2 \tag{3.45}$$

Our single-particle states are defined using a HO basis to get an explicit formula for the one-body density matrix elements:

$$\phi_i(\vec{r}) = \psi_{nlm}(\vec{r})\chi_{si}\chi_{ti} \tag{3.46}$$

Where $i = n, l, m, s_i, t_i$ while $\psi_{nlm}(\vec{r})$, χ_{si}, and χ_{ti} are space, spin, and isospin wave functions, respectively. The space wave function of HO is given by:

$$\psi_{nlm}(\vec{r}) = R_{nl}(r)Y_{lm}(\theta_i, \phi_i) \tag{3.47}$$

The equation (3.45) can be written as[70]:

$$\rho_o(r) = \sum_{nlm} |\psi(\vec{r})|^2 . \sum_{s_i,t_i} |\chi_{si}\chi_{ti}|^2 \tag{3.48}$$

$$\rho_o(r) = \sum_{nlm} |R_{nl}(r)Y_{lm}(\theta_i, \phi_i)|^2 . \sum_{s_i,t_i} |\chi_{si}\chi_{ti}|^2 \tag{3.49}$$

$$\rho_o(r) = 4\sum_{nl} |R_{nl}(r)|^2 . \sum_{m} |Y_{lm}(\theta_i, \phi_i)|^2 \tag{3.50}$$

where the factor 4 in equation (3.50) takes into account the spin-isospin degeneracy i.e., The charge density distribution does not depend on the s_i and t_i, therefore these indices have been neglected by summing over the projections m_s and m_t to obtain the factor 4. The second factor of equation (3.50) can be written as[70]:

$$\sum_{m} |Y_{lm}(\theta_i, \phi_i)|^2 = \frac{2l+1}{4\pi} \tag{3.51}$$

The density of the system A nucleons written as[70]:

$$\rho_o(r) = 4\sum_{nl} |R_{nl}(r)|^2 \frac{2l+1}{4\pi} \tag{3.52}$$

Nuclei with Z=N and a closed shell have their ground charge density distributed is given by[70]:

$$\rho_o(r) = 2\sum_{nl} \frac{2l+1}{4\pi} |R_{nl}(r)|^2 \tag{3.53}$$

The ground charge density distribution for open-shell nuclei can be expressed as:

$$\rho_o(r) = \frac{1}{4\pi}\sum_{nl\in I} 2(2l+1)|R_{nl}(r)|^2 + \frac{1}{4\pi}\sum_{nl\notin I} N_p|R_{nl}(r)|^2 \tag{3.54}$$

Where I, N_p are closed shell, number of protons in the unfilled orbit's and $R_{nl}(r)$ is given by:

$$\begin{aligned} R_{nl}(r) =& \frac{1}{(2l+1)!!}[\frac{2^{l-n+3}(2n+2l-1)!!}{b^3\sqrt{\pi}(n-1)!}]^{1/2}\,(r/b)^l\, e^{-r^2/b^2} \\ & {}_1F_1(1-n, l+\frac{3}{2}; \frac{r^2}{b^2}) \end{aligned} \tag{3.55}$$

${}_1F_1(1-n, l+\frac{3}{2}; \frac{r^2}{b^2})$ is the confluent hyper-geometric series and is given by[70]:

$${}_1F_1(1-n, l+\frac{3}{2}; \frac{r^2}{b^2}) = \sum_{k=1}^{n-1}(-1)^k \frac{(n-1)!2^k}{(n-k-1)!k!}\frac{(2l+1)!!}{(2l+2k+1)!!}(r/b)^{2k} \tag{3.56}$$

With n!!=n(n-1)(n-4)....(2 or 1)
n!=n(n-1)(n-2)....1
b is the harmonic oscillator size parameter is given by[70]:

$$b = 1.005A^{1/6}\ \ fm \tag{3.57}$$

Size parameter b is dependent on the nuclear mass number A, which is the case for HO wells.

Chapter Four
Results and Discussion

4.1 Introduction

The electron scattering calculations have studied the longitudinal form factor in the present over the momentum transfer or effect momentum transfer ranges ($0 \leq q$ or $q_{eff} \leq 3$). The shell model calculation was performed using Nushell codes for Windows [82] within extended sdpf-model space. All the calculations are performed using sdpfnow as a residual effective interaction within a restricted model space is one of the models, which succeeded in describing the static properties of nuclei with effective charges are used. In this work, ^{16}O nucleus was used as the inert core and we used the Bohr-Mottelson (BM) collective model to calculated the electron scattering form factors on sdpf-model space for ^{31}P, ^{27}Al, ^{23}Na and ^{24}Mg nuclei. The HO, WS and SKX potential have been used to calculate the wave functions of the single-particle matrix elements. In this calculations the experimental data represent by black point, the SK potential represent by brown solid curve, the WS potentials represent by the blue dashed curve, and HO potential represent by the forest green doted curve. The proton and neutron effective charges from the table (4.1). The OBDM elements used in present work are calculated by generating the wave functions of a given transition in the know nuclei from Nushell that contains the complete library of shell model effective interaction.

4.2 The nucleus ^{31}P

Phosphorous (P) has twenty-three known isotopes with mass numbers between ^{24}p and ^{46}p nuclei. Of these isotopes, only one stable isotope ^{31}P nucleus. The phosphorous nucleus contains 15 protons and 16 neutrons. The core used of ^{31}P nucleus is ^{16}O nucleus. The valance nucleons distributed on $(1d_{5/2}, 1d_{1/2}, 2s_{1/2}, 1f_{7/2}, 2p_{3/2})$. The ^{31}P nucleus has electric quadrupole moments Q equals to $0.04fm^2$ [83]. Figure (4.1) shows the relation between longitudinal form factor $F(q)$ and moment transfer q. In this figure, the theoretical result of the ^{31}P nucleons is compared with the experimental data in the region ($0 \leq q \leq 3$). The theoretical consequence of C0 transition for ^{31}P nucleus (J_i^π $T = 1/2^+$ $1/2$) With (WS) potential good agreement with the experimental result in the first

Table 4.1: The proton and neutron effective charges

Nuclei	e_P	e_n
^{31}P	3.5e	2.5e
^{23}Na	1.35e	0.35e
^{27}Al (5/2 to $1/2_2$)	1.16e	0.78e
^{27}Al (5/2 to $3/2_2$)	1.16e	0.78e
^{27}Al (5/2 to 7/2)	1.16e	0.78e
^{25}Mg (5/2 to $1/2_2$)	1.5e	0.5e
^{25}Mg (5/2 to $3/2_2$)	7.5e	7.5e
^{25}Mg (5/2 to $5/2_2$)	0.01e	0.01e
^{25}Mg (5/2 to 7/2)	1.05e	0.30e
^{25}Mg (5/2 to 9/2)	0.35e	0.35e
^{25}Mg (5/2 to $9/2_2$)	1e	0.35e
^{25}Mg (5/2 to 11/2)	1.001e	0.001e

and second maximum momentum transfer. The theoretical consequence of ^{31}P nucleus with (HO) potential with size parameter b=1.78 fm was obtained using the equation (3.57) approximation is in agreement with the experimental result. The electron scattering form factor results with (HO) potential shifted the calculations toward increased the momentum transfer on the second and third maximum momentum transfer region. But the theoretical consequence of ^{31}P nucleus with (SKX) potential is in excellent agreement with the experimental result on the first, second, and third maximum momentum transfer. These calculations were performed using Bohr-Mottelson and all theoretical results more close to experimental data.[84].

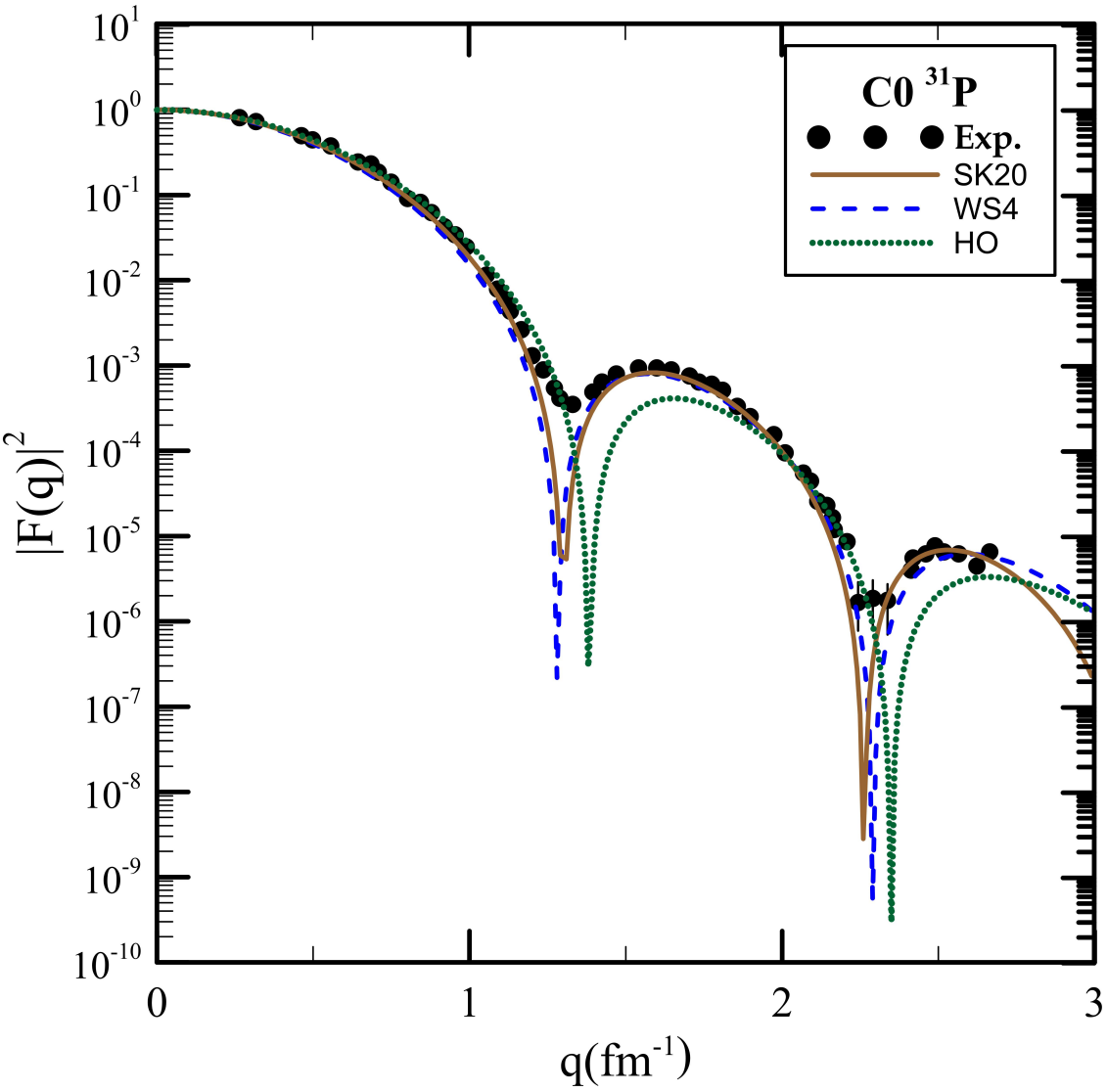

Figure 4.1: The relation between moment transfer q and longitudinal C0 form factor $F(q)$ for ^{31}P nucleus. All curves represent the calculation Bohr-Mottelson (BM) collective model with SKX, HO and WS potentials.

4.3 The nucleus ^{23}Na

Sodium has twenty known isotopes. The isotope sodium-23 is the only stable isotope, so sodium is a mono-atomic element. The ^{23}Na nucleus has 11 protons (atomic number) and 12 neutrons. The ^{23}Na nucleus has electric quadrupole moments Q equals to $10.45fm^2$ [85].
The longitudinal form factors (C0+C2) for the $3/2^+$ state of the ^{23}Na nucleus calculated on the sdpf-shells model with the sdpfnow as residual effective interaction and Harmonic Oscillator (HO) as potential with size parameter $b = 1.69fm$ was obtained using the equation (3.57) to calculate the wave functions of the radial single particle-matrix element shown in Fig (4.2). The blue dashed curve represents the theoretical calculation of C0 longitudinal form factors, and C2 represent the grass green dashed dotted. The forest green solid curve represents the C0+C2 form factors and sold curve in agreement with the experimental result in region $0 \leq q \leq 1$ on the first maximum momentum transfer and region $1.4 \leq q \leq 1.7$. The calculations with WS and SKX potentials are failed to described the experimental data. The experimental data are taken from Ref [86].

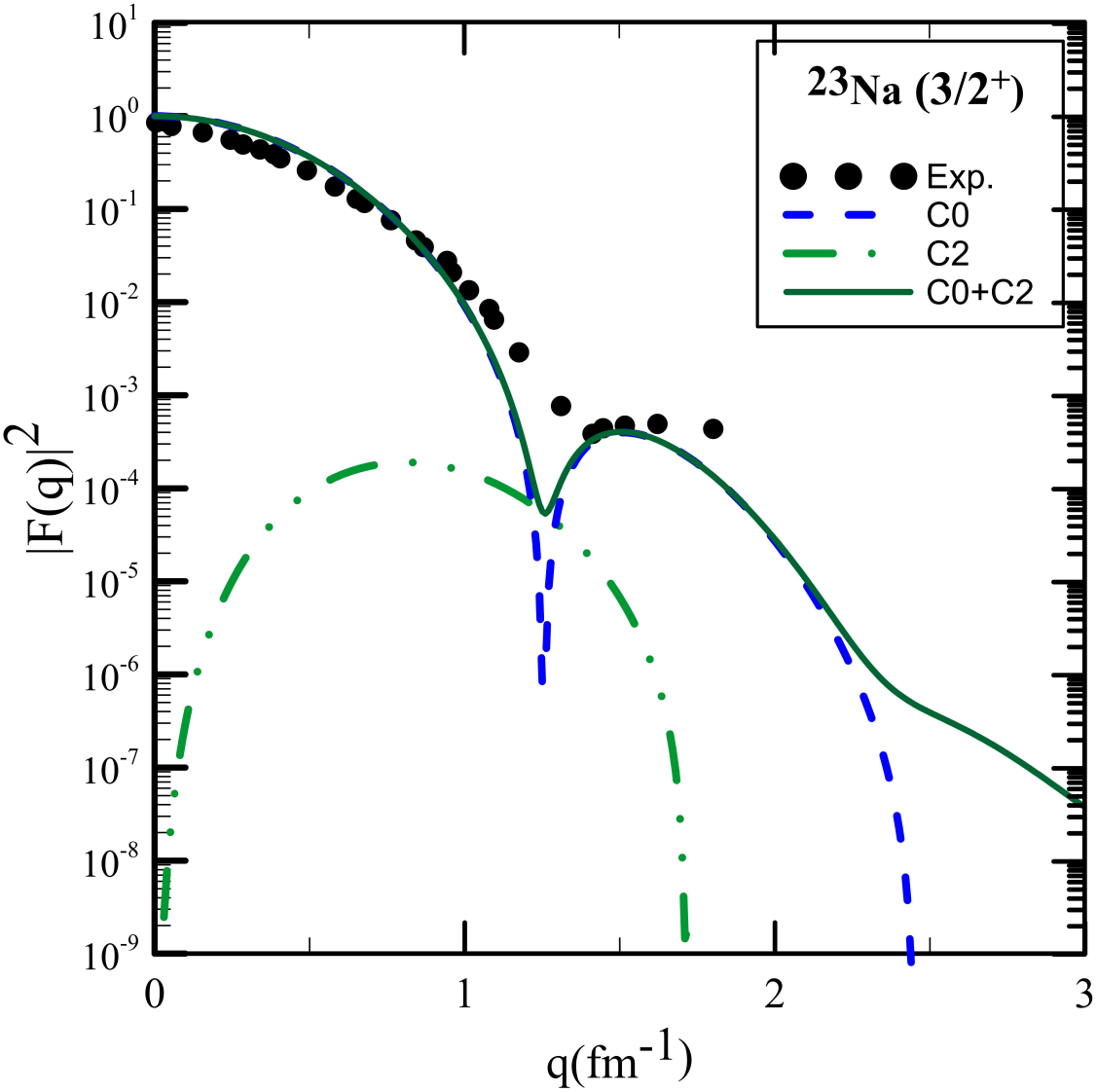

Figure 4.2: The relation between moment transfer q and longitudinal C0, C2, and C0+C2 form factors $F(q)$ for ^{23}Na nucleus. All curves represent the calculation Bohr-Mottelson (BM) collective model with Harmonic Oscillator (HO) potential.

4.4 The nucleus ^{27}Al

The ^{27}Al nucleus has 13 protons and 14 neutrons. The ^{27}Al nucleus has 11 particles outside the core. The experiment data for ^{27}Al nucleus taken from the ref [87]. The ^{27}Al nucleus has electric quadrupole moments Q equals to $14.66fm^2$ [85].

4.4.1 The longitudinal form factor for $1/2_2^+$ 1/2 state

Fig (4.3) shows the relation between longitudinal form factor $F(q)$ and effective moment transfer q_{eff}. In this figure, the theoretical result of the ^{27}Al nucleus are compared with experimental result in the region $0 \leq q_{eff} \leq 3$. The theoretical result of C2 transition for ^{27}Al nucleus. $(J_i^\pi\ T = 5/2^+\ 1/2)$ to $(J_i^\pi\ T = 1/2_2^+\ 1/2)$ With WS potential agreement with the experimental result in region $0.5 \leq q_{eff} \leq 1.2$ on the first maximum effective momentum transfer but in region $1.2 \leq q_{eff} \leq 1.8$ and in region $2 \leq q_{eff}$ do not agree with experimental result and increases the highest practical values. The theoretical result of ^{27}Al nucleus with HO potential with b=1.74 was obtained using the equation (3.57) agreement with the experimental result in region $0.8 \leq q_{eff} \leq 1.4$ first maximum effective momentum transfer. The theoretical result of ^{27}Al nucleus with SKX potential good agreement with experimental result in region $0.5 \leq q_{eff} \leq 1.3$ and $2 \leq q$.

4.4.2 The longitudinal form factor for $3/2_2^+$ 1/2 state

Fig (4.4) shows the relation between longitudinal form factor $F(q)$ and effective moment transfer q_{eff}. In this figure, the theoretical result of the ^{27}Al nucleus are compared with experimental result in the region $0 \leq q_{eff} \leq 3$. The theoretical result of C2 transition for ^{27}Al nucleus. $(J_i^\pi\ T = 5/2^+\ 1/2)$ to $(J_i^\pi\ T = 3/2_2^+\ 1/2)$ with SKX potential agreement with experimental result in region $0.5 \leq q_{eff} \leq 1.4$ on the first maximum effective momentum transfer and approximation agreement with experimental result in region $2.1 \leq q_{eff}$. The brown sold curve represent the theoretical result with HO potential with b=1.74 was obtained using the equation (3.57) agreement with experimental result in region $q_{eff} \leq 2$ but not good agreement in region $2 \leq q_{eff}$. The theo-

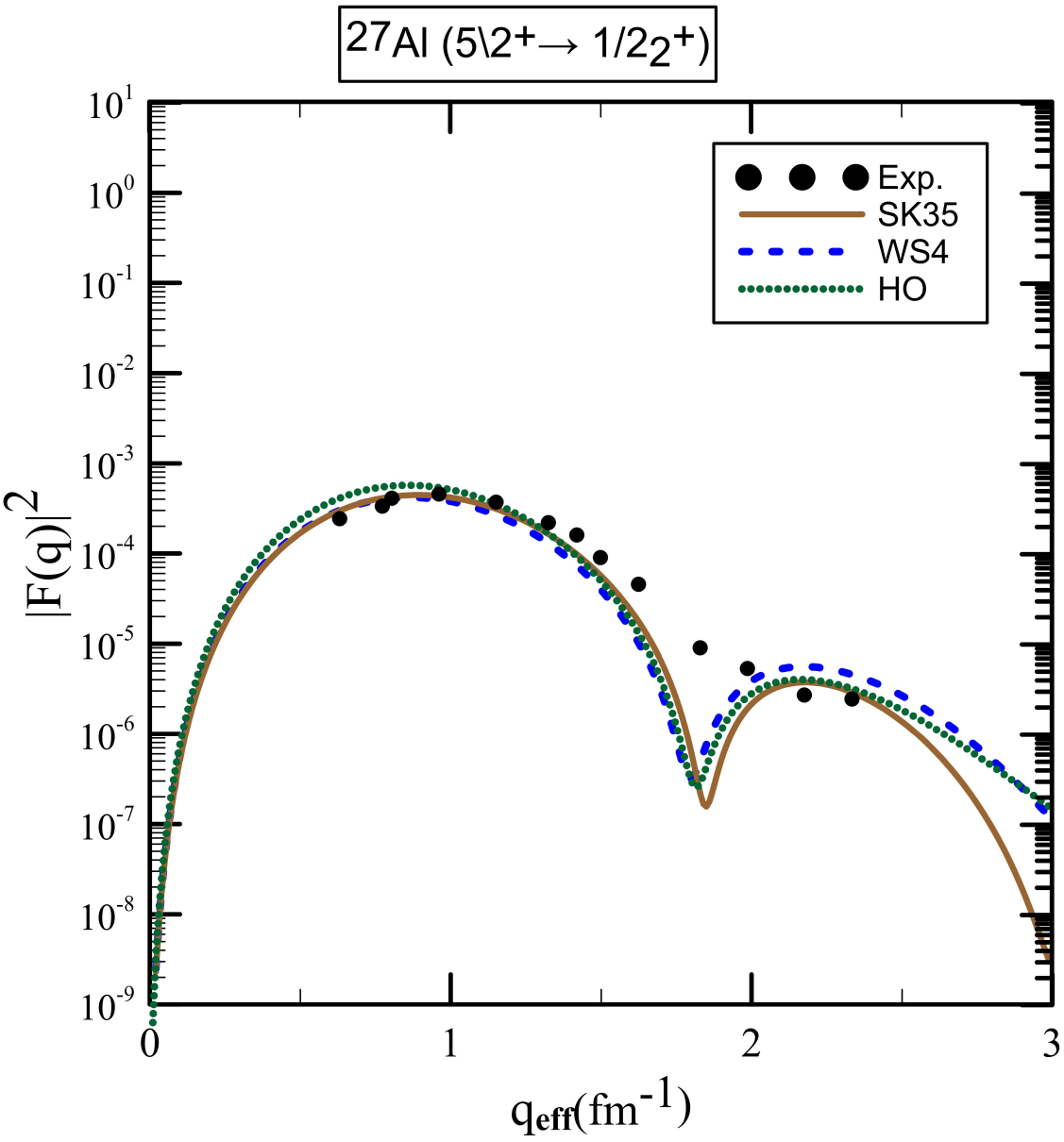

Figure 4.3: The relation between effective moment transfer q_{eff} and longitudinal C2 form factor $F(q)$ for ^{27}Al nucleus. All curves represent the calculation Bohr-Mottelson (BM) collective model with SKX, HO and WS potentials.

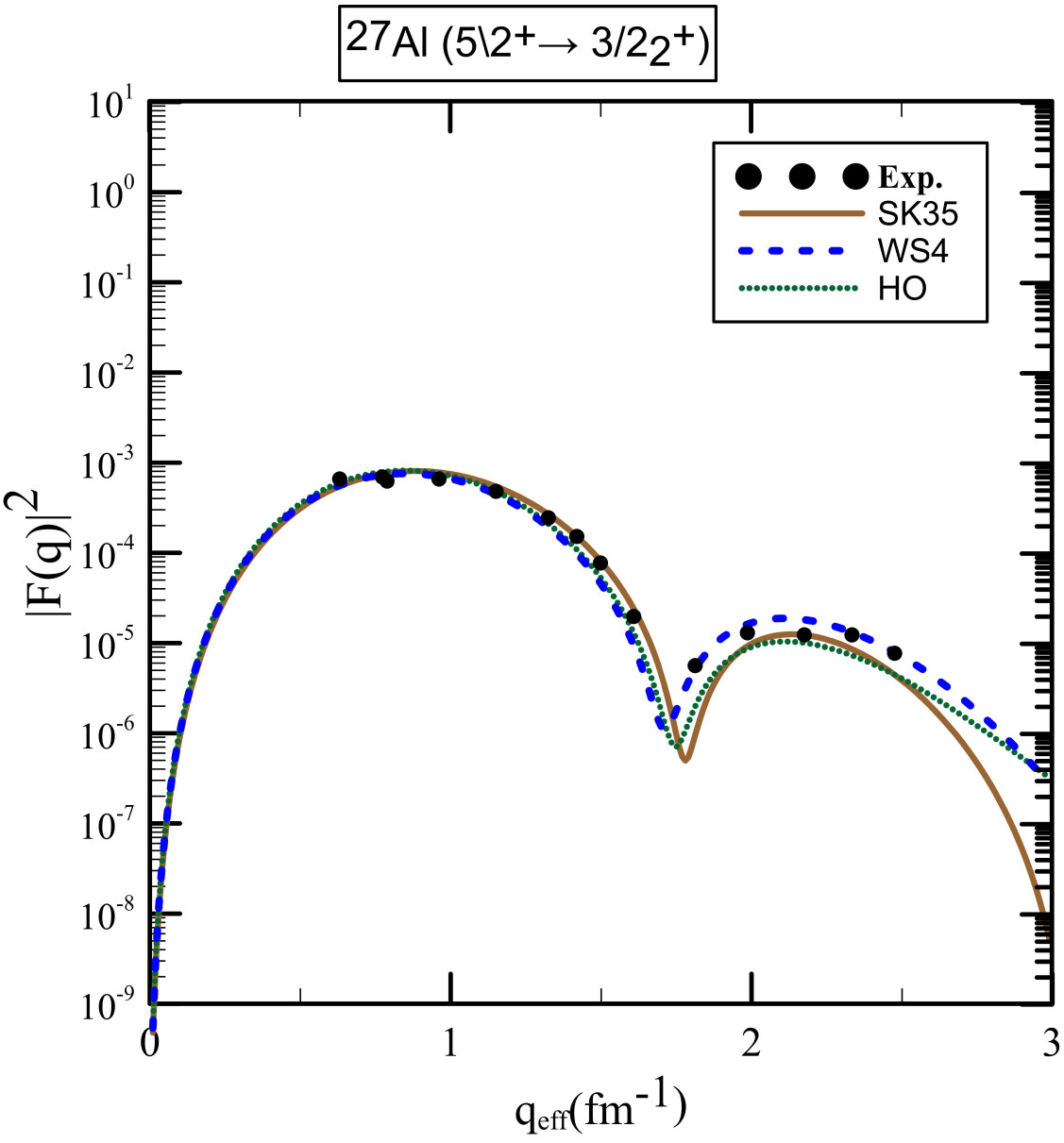

Figure 4.4: The relation between effective moment transfer q_{eff} and longitudinal C2 form factor $F(q)$ for ^{27}Al nucleus. All curves represent the calculation Bohr-Mottelson (BM) collective model with SKX, HO and WS potentials.

retical data with WS potential good agreement with the experimental result on the first and second maximum effective momentum transfer.

4.4.3 The longitudinal form factor for $7/2^+$ 1/2 state

Fig (4.5) shows the relation between longitudinal form factor $F(q)$ and effective moment transfer (q_{eff}). In this figure, the theoretical result of the ^{27}Al nucleus are compared with experimental result in the region $0 \leq q_{eff} \leq 3$. The theoretical result of C2 and C4 transition for ^{27}Al.(J_i^π $T = 5/2^+$ $1/2$) to (J_i^π $T = 7/2^+$ $1/2$) with WS potential. The theoretical calculation of C2 longitudinal form factors represent by the dark blue dashed curve good agreement with experimental result in region $0.5 \leq q \leq 2$ on the first maximum momentum effective transfer but on second maximum momentum effective transfer the curve up the experiments data, the C4 represent by the twilight blue dashed dotted curve, and also the C2+C4 longitudinal form factors represent by the blue solid curve good agreement in the same region as the first maximum momentum effective transfer.

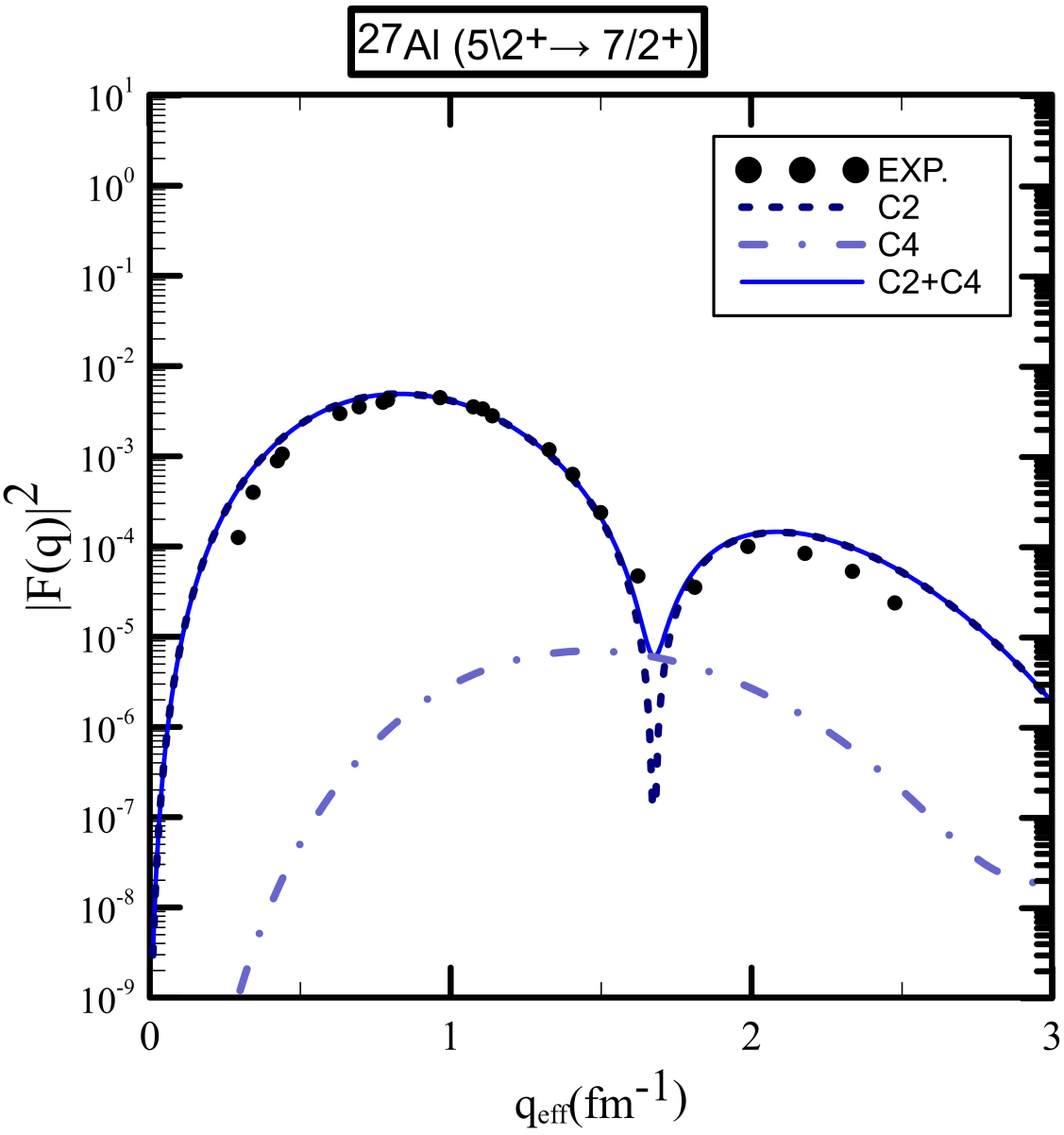

Figure 4.5: The relation between effective moment transfer (q_{eff}) and longitudinal C2, C4, and C2+C4 form factors $F(q)$ for ^{27}Al nucleus. All curves represent the calculation Bohr-Mottelson (BM) collective model with WS4 potential.

4.5 The nucleus ^{25}Mg

The Magnesium nucleus has 21 known isotopes, but only three of these isotopes ($^{24-26}Mg$) nuclei are stable. The nucleus of the isotope ^{25}Mg contains 12 protons and 13 neutrons. In the nuclear shell model, the crusts are filled with nucleons in an increasing order with respect to energy when moving to higher crusts, as they represent the paired nucleons inert core represents the filled shells, while the nucleons outside the core represent the valence nucleons. ^{25}Mg nucleus imagined as composed of tightly bound core ^{16}O nucleus plus nine loosely bound nucleons outside the core was split of sdpf-shell. All the calculation were performed using NuShell with the SKX potential, WS potential, and HO potential with b=1.718 was obtained from the equation (3.57). The experimental data are taken from ref[88]. The ^{25}Mg nucleus has electric quadrupole moments Q equals to $19.92fm^2$ [85].

4.5.1 Form factor for the $5/2 \rightarrow 1/2_2$ transition

A comparison between the experimental and theoretical form factors with the SKX, WS and, HO potentials for the C2 transition for ^{25}Mg nucleus is given in figure (4.6). The first momentum maximum of longitudinal electrical transition form factors occurs at $0.89fm^{-1}$ momentum transfer, and we observe that the theoretical are in agreement with experimental data in the region from $0.4 \leq q_{eff} \leq 1.4fm^{-1}$ so by using C2, a match was achieved between practical and theoretical values. The curves of SKX, WS, and HO potentials are close to the practical results on the first momentum maximum, but on the second momentum maximum the curve separated from each other. The SKX potential is better slightly than other potential.

4.5.2 Form factor for the $5/2 \rightarrow 3/2_2$ transition

For scattered electron leaves the nucleus in the ground-state has($J^\pi T = 5/2\ {}^-1/2$) with $E = 0.0$ Mev and the excited state ($J^\pi T = 3/2_2\ {}^-1/2$) with $E = 2.801$ Mev. The first effective momentum maximum of longitudinal electrical transition form factors occurs at $0.88fm^{-1}$ effective momentum transfer in figure (4.7). On the first effective momentum

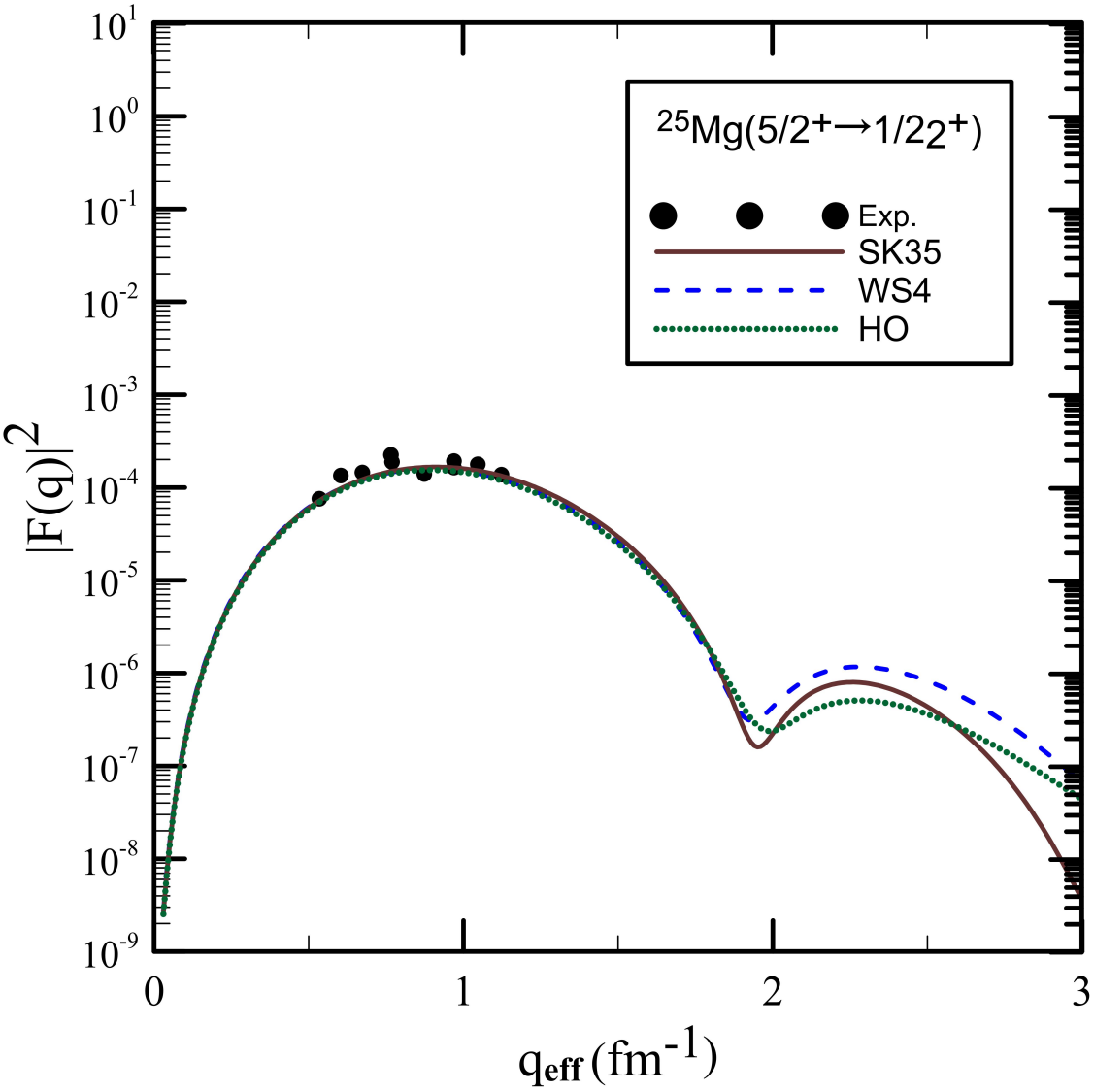

Figure 4.6: The relation between effective moment transfer q_{eff} and longitudinal C2 form factor $F(q)$ for ^{25}Mg nucleus. The curves represent the calculation Bohr-Mottelson (BM) collective model with the SKX, WS, and HO potentials.

maximum the three curves approximate each other and correspond to the experimental results, but on the second effective momentum maximum The three curves diverge from each other.The SKX potential is better slightly than other potential.
In the figure (4.8) the results dark brown dashed curve represent C2 transition, the red brown dashed doted curve represent C4 transition, and the brown solid curve represent C2+C4 transition are closer to the experimental data.[88] There is a good match between the theoretical and practical values within the limits of region $0.5 \leq q_{eff} \leq 1.3fm^{-1}$. The inelastic form factor calculations were completed with SKX potential.

4.5.3 Form factor for the $5/2 \rightarrow 5/2_2$ transition

The figure (4.9) shows the results of longitudinal form factor with the SKX, WS, and HO potentials. All the curves approximately agreement with the experimental data, but the blue dashed curve with WS is best agreement on the first effective momentum maximum.
The C2 and C4 form factors for the ($5/2\ ^-1/2$) ground state at 1.964 Mev are shown in Figure (4.10). The result with using BM collective model with WS potential is closer to the data of Ref.[88] The C2 represent by the dark blue dashed curve, the C4 represent by the twilight blue dashed dotted curve, and C2+C4 represent by blue solid curve. There is a good match between the theoretical and experimental data.

4.5.4 Form factor for the $5/2 \rightarrow 7/2$ transition

The theoretical results in the figure (4.11) agreement with the experimental data in the first effective momentum maximum. The blue dashed curve with WS potential and the green dotted HO potential match better than brown solid curve with SKX potential.
The calculation for the C2 and C4 longitudinal for the transitions from the ($5/2\ ^-1/2$) ground state to the ($7/2\ ^-1/2$) with WS potential in figure (4.12). The dark blue dashed curve represent the C2 longitudinal, the twilight blue dashed dotted curve represent C4 longitudinal, and the blue solid curve is C2+C4. The Theoretical data of (C2+C4) agreement with the experimental data on the first effective momentum maximum.

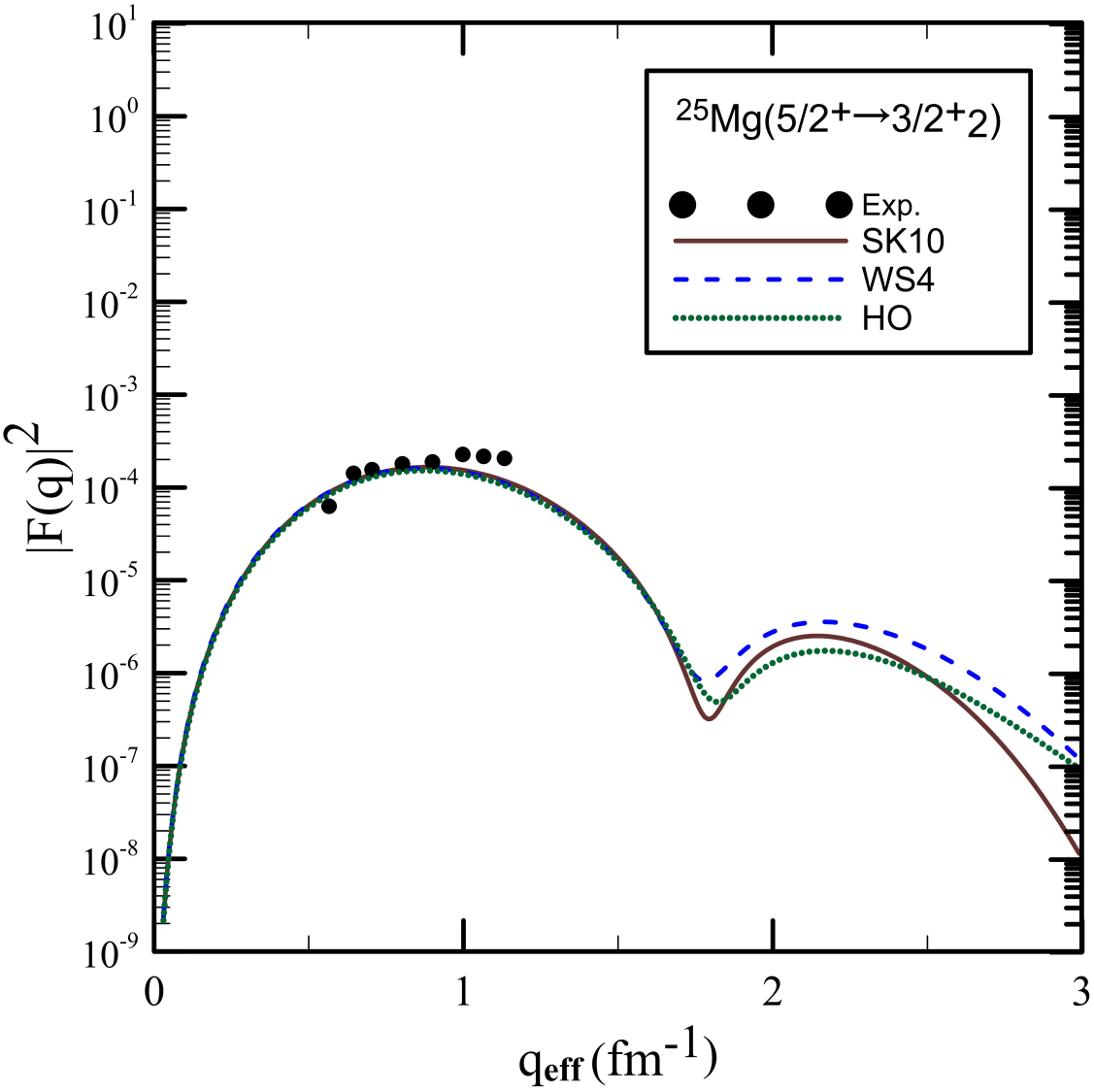

Figure 4.7: The relation between effective moment transfer q_{eff} and longitudinal C2 form factor $F(q)$ for ^{25}Mg nucleus. The curves represent the calculation Bohr-Mottelson (BM) collective model with SKX, WS, and HO potentials.

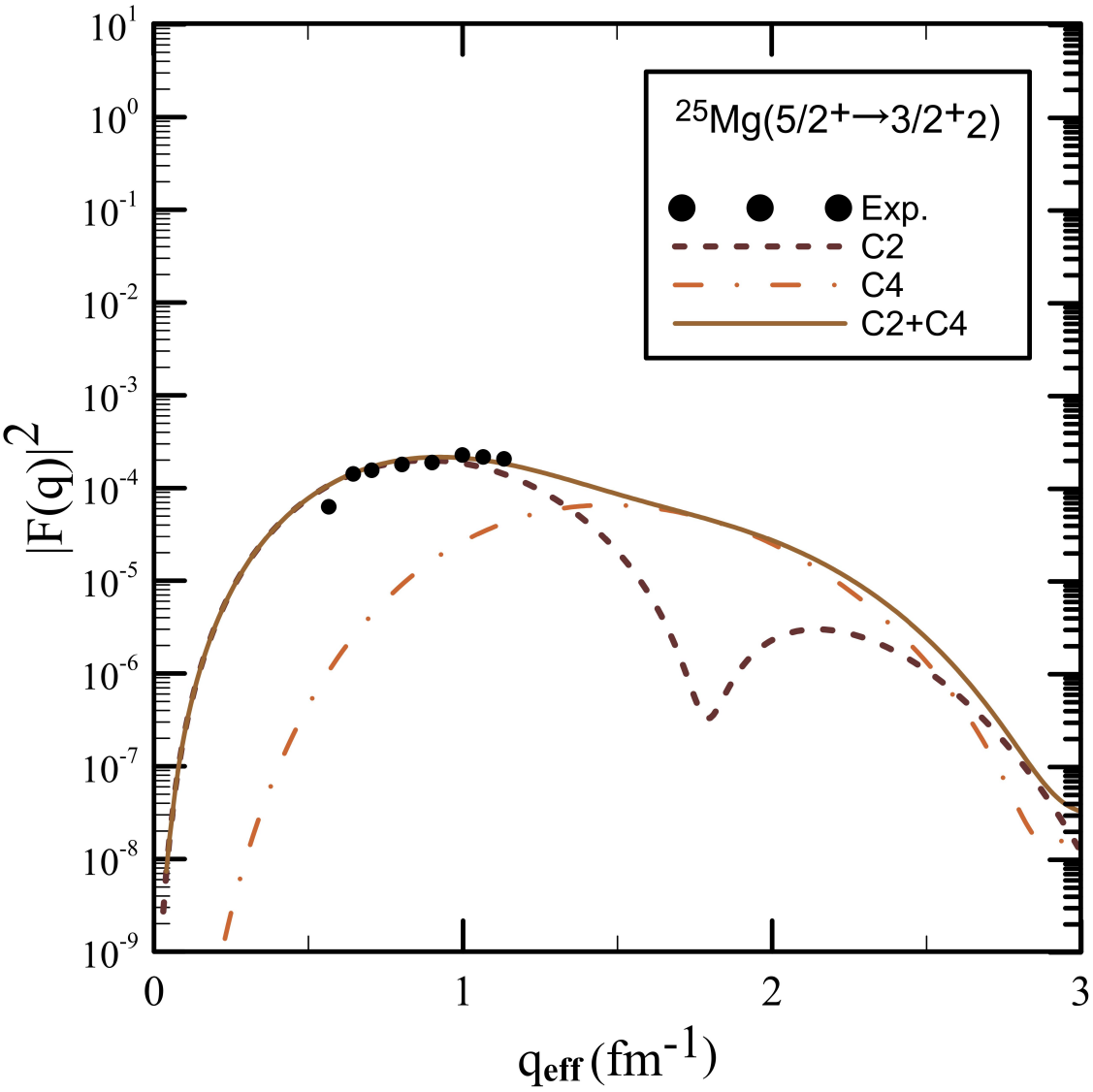

Figure 4.8: The relation between moment transfer q_{eff} and longitudinal C2, C4, and C2+C4 form factors $F(q)$ for ^{25}Mg nucleus. All curves represent the calculation Bohr-Mottelson (BM) collective model with SKX potential.

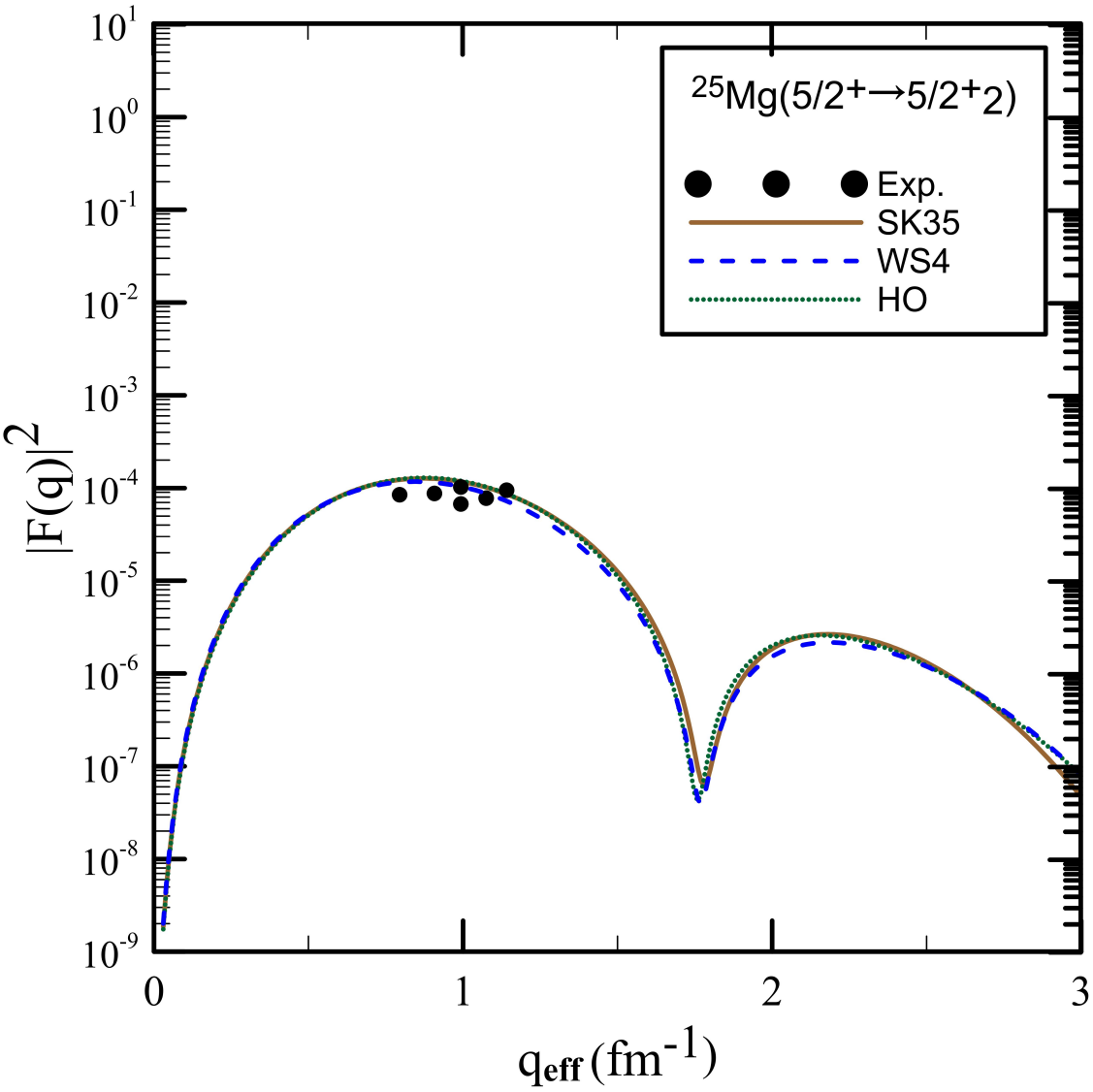

Figure 4.9: The relation between effective moment transfer q_{eff} and longitudinal C2 form factor $F(q)$ for ^{25}Mg nucleus. The curves represent the calculation Bohr-Mottelson (BM) collective model with SKX, WS, and HO potentials.

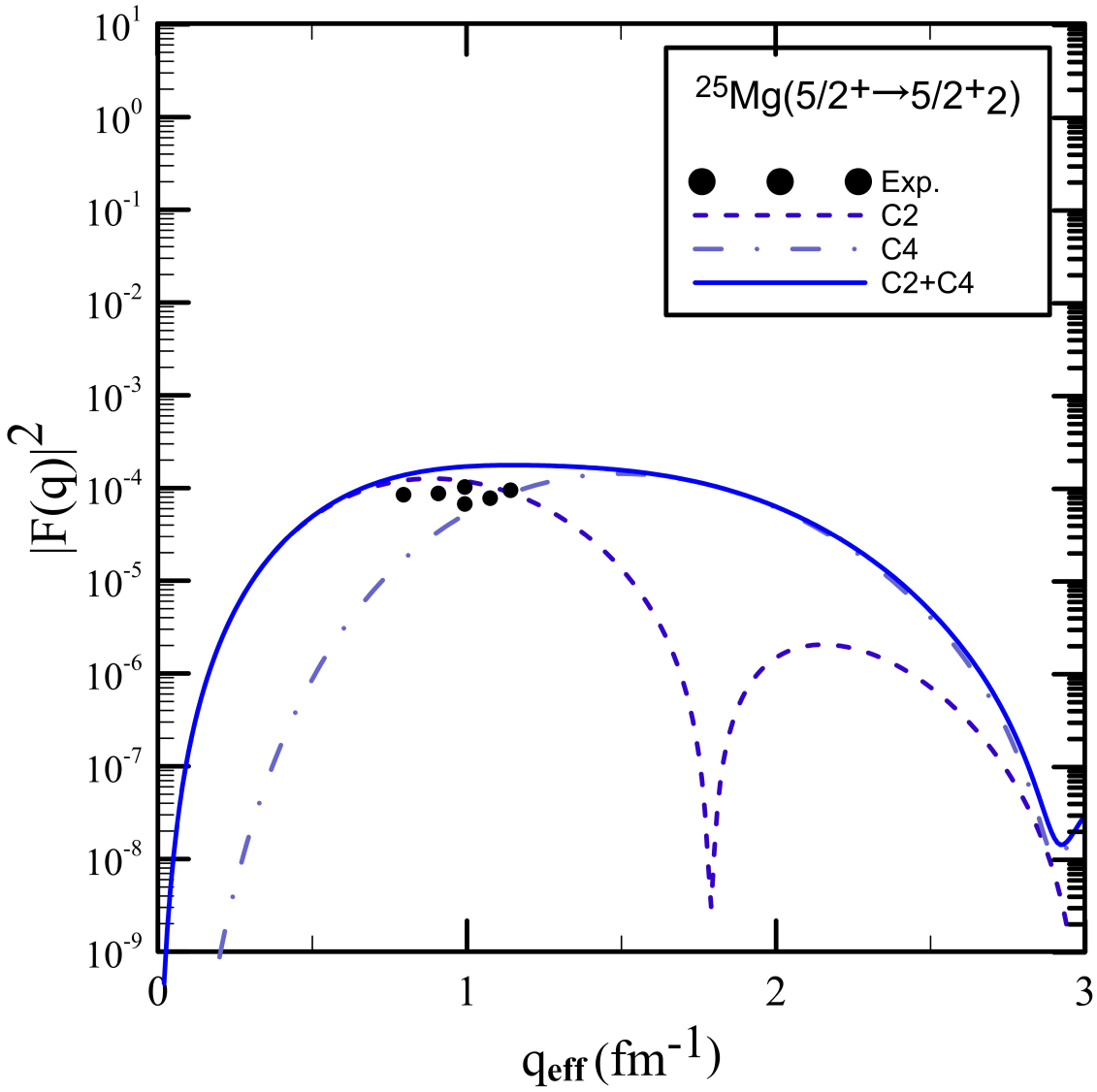

Figure 4.10: The relation between effective moment transfer q_{eff} and longitudinal C2, C4, and C2+C4 form factors $F(q)$ for ^{25}Mg nucleus. All curves represent the calculation Bohr-Mottelson (BM) collective model with WS potential.

4.5.5 Form factor for the $5/2 \rightarrow 9/2$ transition

The all curves in figure (4.13) in the first effective momentum maximum agreement with the experimentally date. The WS potential is better slightly than other potential.
Figure (4.14) represent the longitudinal C2 and C4 for the transitions from the ($5/2\ ^{-}1/2$) ground state to the ($9/2\ ^{-}1/2$) in figure (4.14). The fp-shell model calculations within including the effect of core polarization by using the effective charge. Bohr-Mottelson model with WS4 potential are used in this calculation. In Figure (4.14) the dark blue dashed line represent C2 longitudinal transition and the twilight blue dashed dotted curve represent C4 longitudinal transition. Theoretical data for C2+C4 represent by blue solid curve are almost identical to the experimental data.

4.5.6 Form factor for the $5/2 \rightarrow 9/2_2$ transition

The first effective momentum maximum in the figure (4.15) contains a good match between the curves and the practical data. The WS potential is better slightly than other potential.
The electron excites the nucleus from the ground state ($5/2\ ^{-}1/2$) to the state ($9/2_2\ ^{-}1/2$) with excitation energy of 4.059 MeV in figure (4.16). The theoretical data is an excellent agreement with experimental data. The dark blue dashed curve is the C2 longitudinal and the Twilight blue dashed dotted curve represent C4 longitudinal. The Coulomb C2+C4 form factors results with BM collective model with WS potential effect have good agreement with data from ref [88].

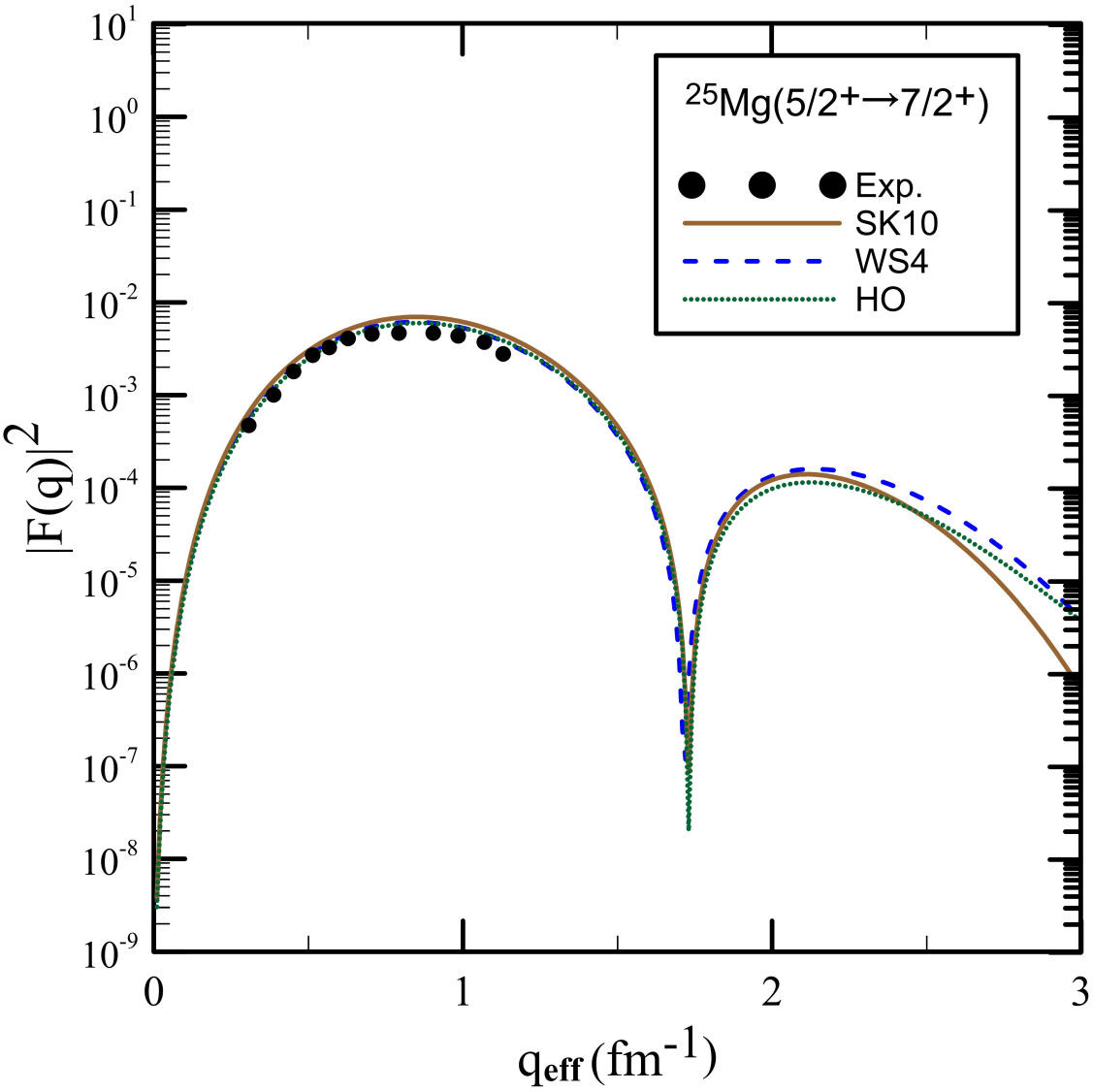

Figure 4.11: The relation between effective moment transfer q_{eff} and longitudinal C2 form factor $F(q)$ for ^{25}Mg nucleus.The curves represent the calculation Bohr-Mottelson (BM) collective model with SKX, WS, and HO potentials.

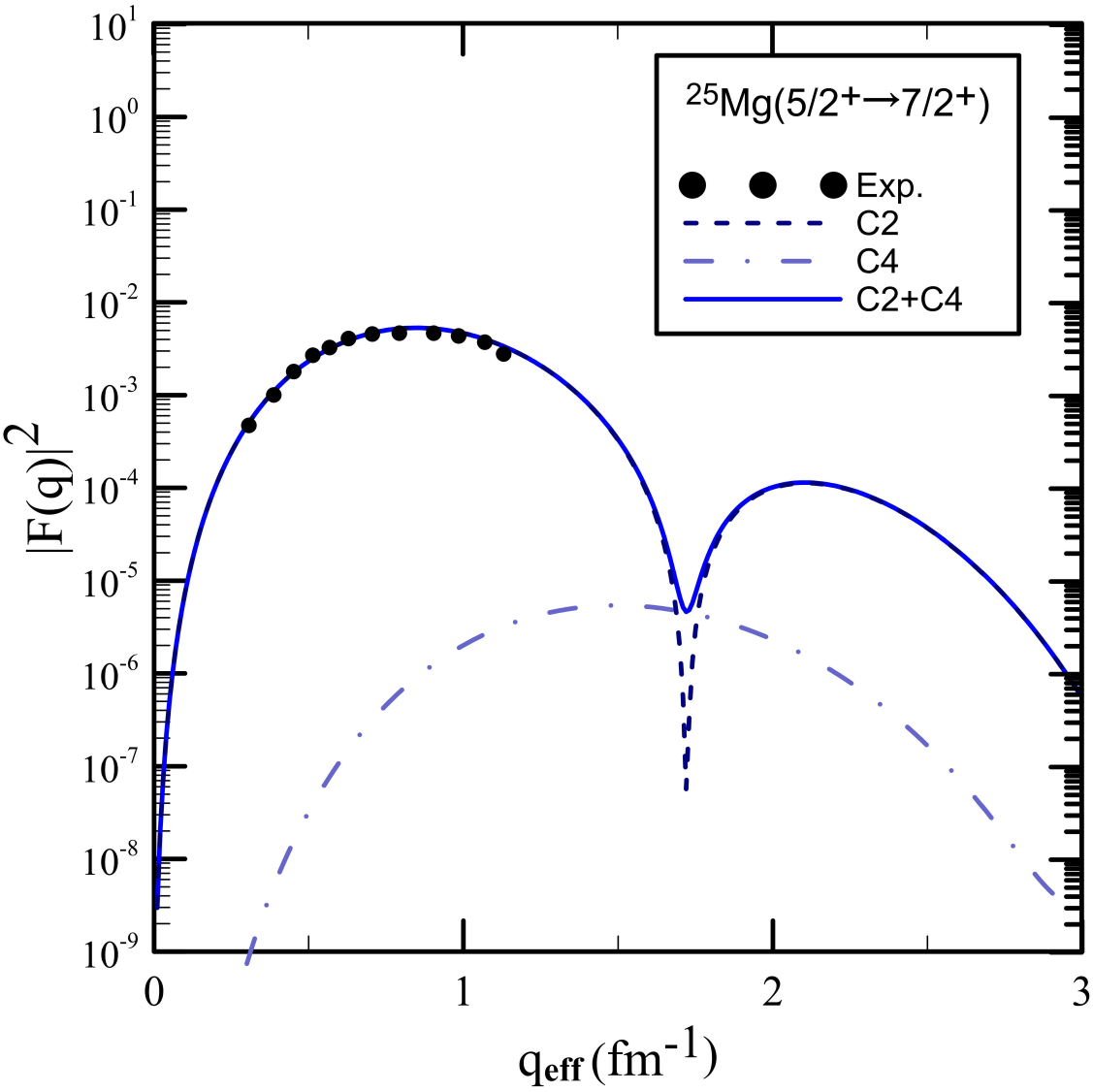

Figure 4.12: The relation between effective moment transfer q_{eff} and longitudinal C2, C4, and C2+C4 form factors $F(q)$ for ^{25}Mg nucleus. All curves represent the calculation Bohr-Mottelson (BM) collective model with Wood-Saxon's potential.

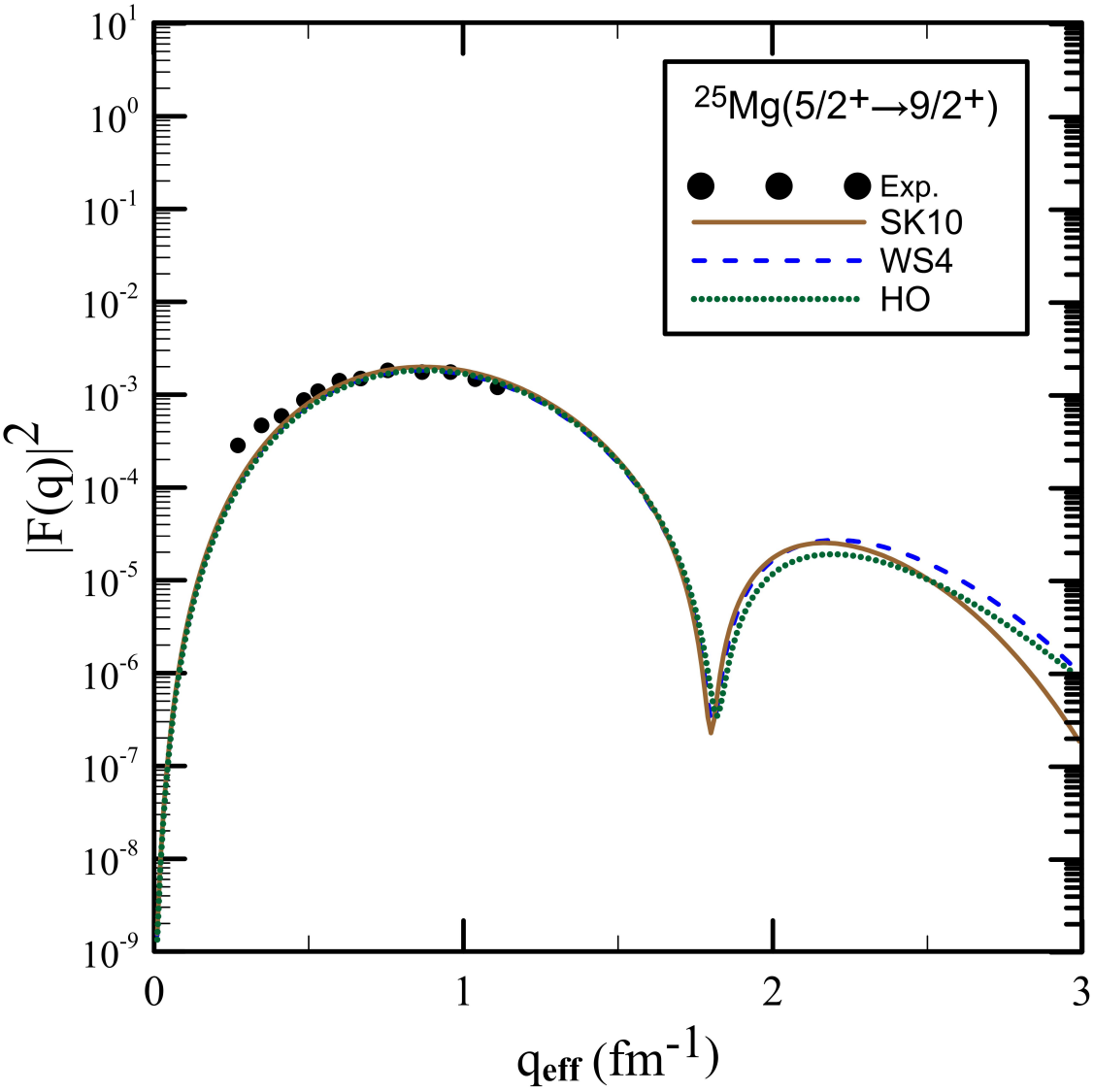

Figure 4.13: The relation between effective moment transfer q_{eff} and longitudinal C2 form factor $F(q)$ for ^{25}Mg nucleus. The curves represent the calculation Bohr-Mottelson (BM) collective model with SKX, WS, and HO potential.

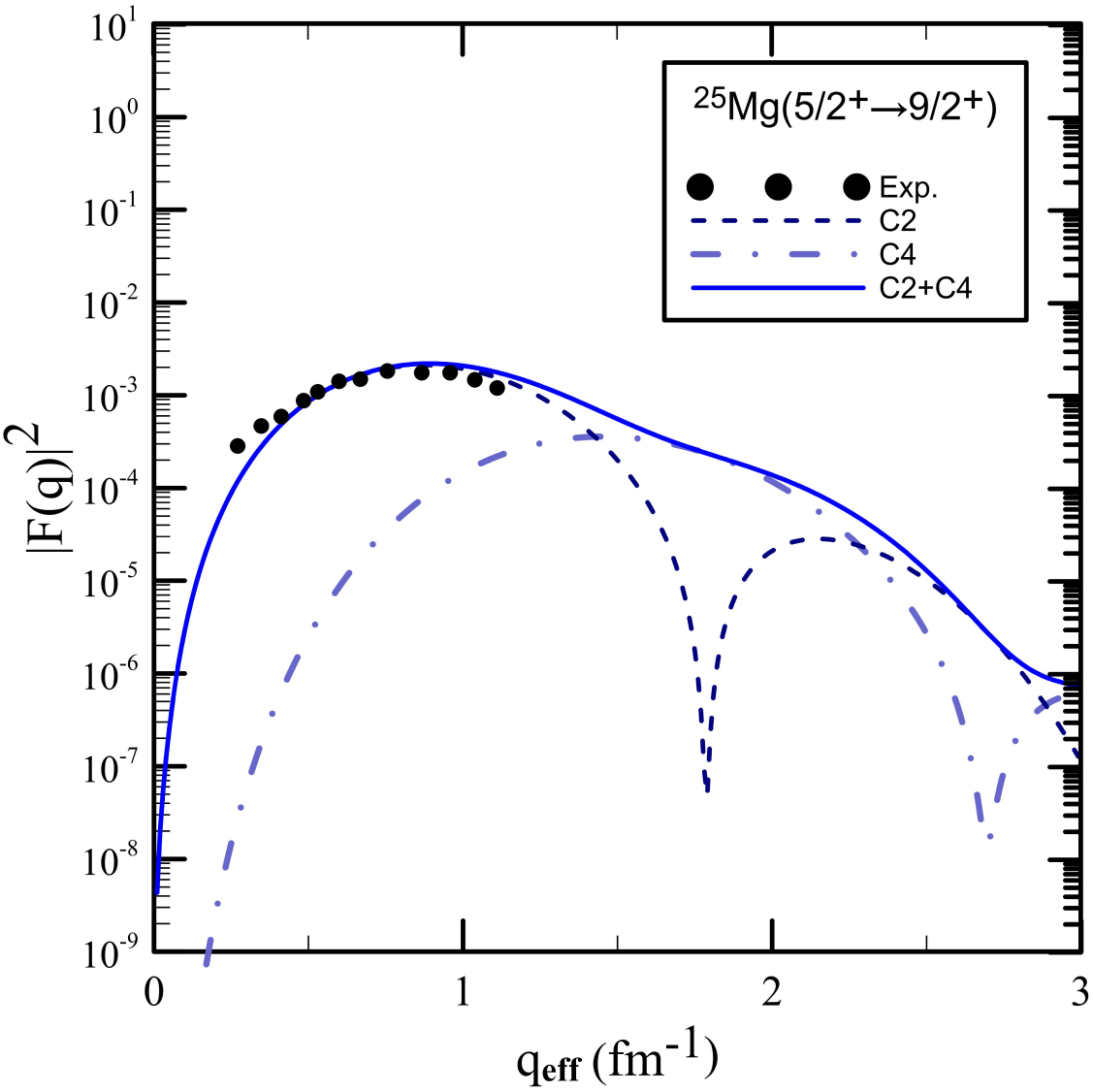

Figure 4.14: The relation between effective moment transfer q_{eff} and longitudinal C2, C4, and C2+C4 form factors $F(q)$ for ^{25}Mg nucleus. All curves represent the calculation Bohr-Mottelson (BM) collective model with WS potential.

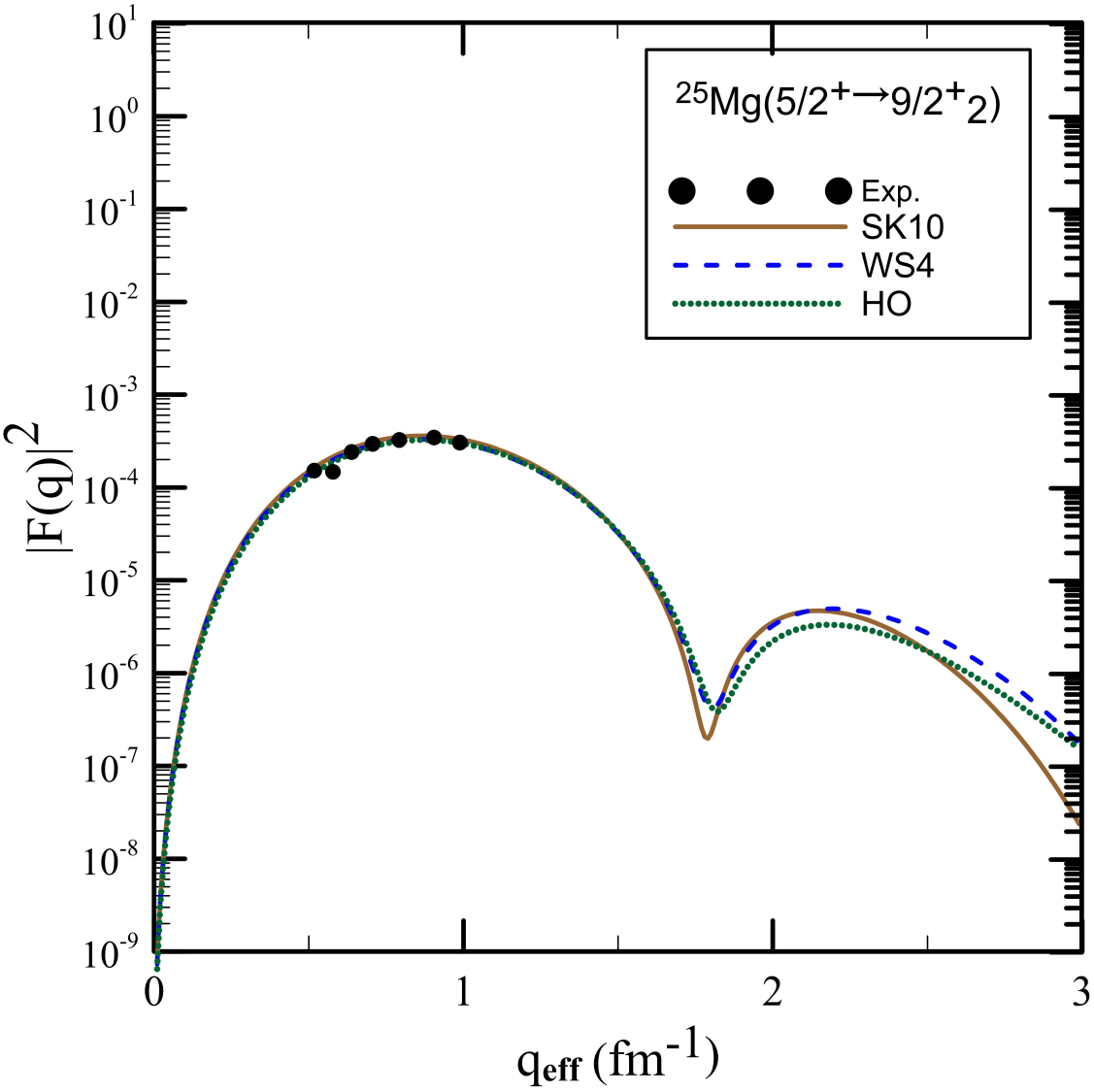

Figure 4.15: The relation between effective moment transfer q_{eff} and longitudinal C2 form factor $F(q)$ for ^{25}Mg nucleus. The curves represent the calculation Bohr-Mottelson (BM) collective model with SKX, WS, and HO potentials.

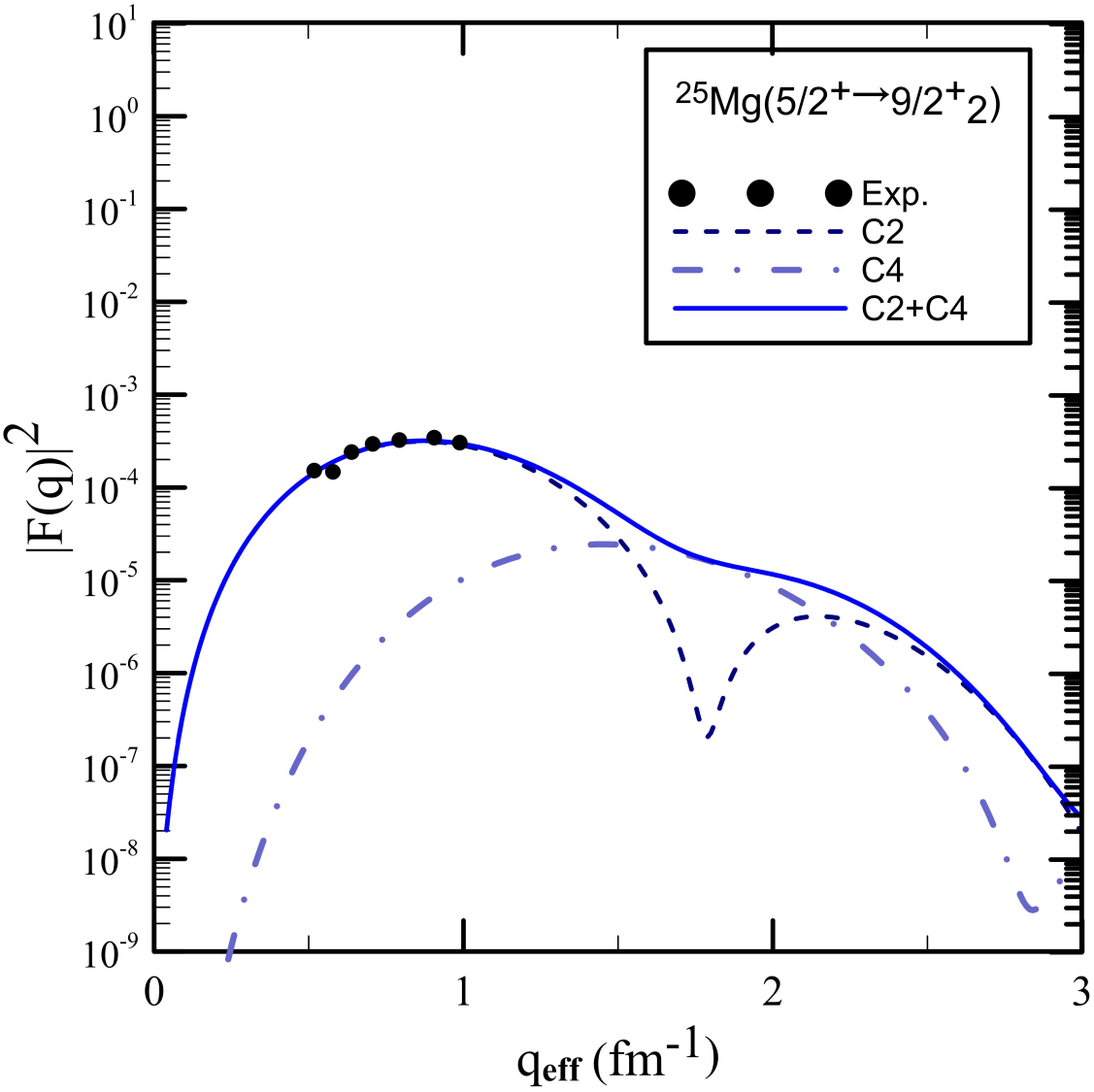

Figure 4.16: The relation between effective moment transfer q_{eff} and longitudinal C2, C4, and C2+C4 form factors $F(q)$ for ^{25}Mg nucleus. All curves represent the calculation Bohr-Mottelson (BM) collective model with WS potential.

Table 4.2: Potentials most consistent with the experimental data

Nuclei	**potentials**
^{31}P	SKX
^{23}Na	HO
^{27}Al (5/2 to $1/2_2$)	SKX
^{27}Al (5/2 to $1/3_2$)	WS
^{27}Al (5/2 to 7/2)	SKX
^{25}Mg (5/2 to $1/2_2$)	SKX
^{25}Mg (5/2 to $3/2_2$)	SKX
^{25}Mg (5/2 to $5/2_2$)	WS
^{25}Mg (5/2 to 7/2)	WS
^{25}Mg (5/2 to 9/2)	WS
^{25}Mg (5/2 to $9/2_2$)	WS
^{25}Mg (5/2 to 11/2)	SKX

4.5.7 Form factor for the $5/2 \rightarrow 11/2$ transition

The electron excites the nucleus from the ground state (5/2 $^{-}$1/2) to the state (11/2 $^{-}$1/2). The coulomb C4 in Figure (4.17) with SKX potential better than the rest of the curves in conformity with the practical values and the WS potential better than HO potential. The longitudinal C4 has almost in agreement with the experimental data.

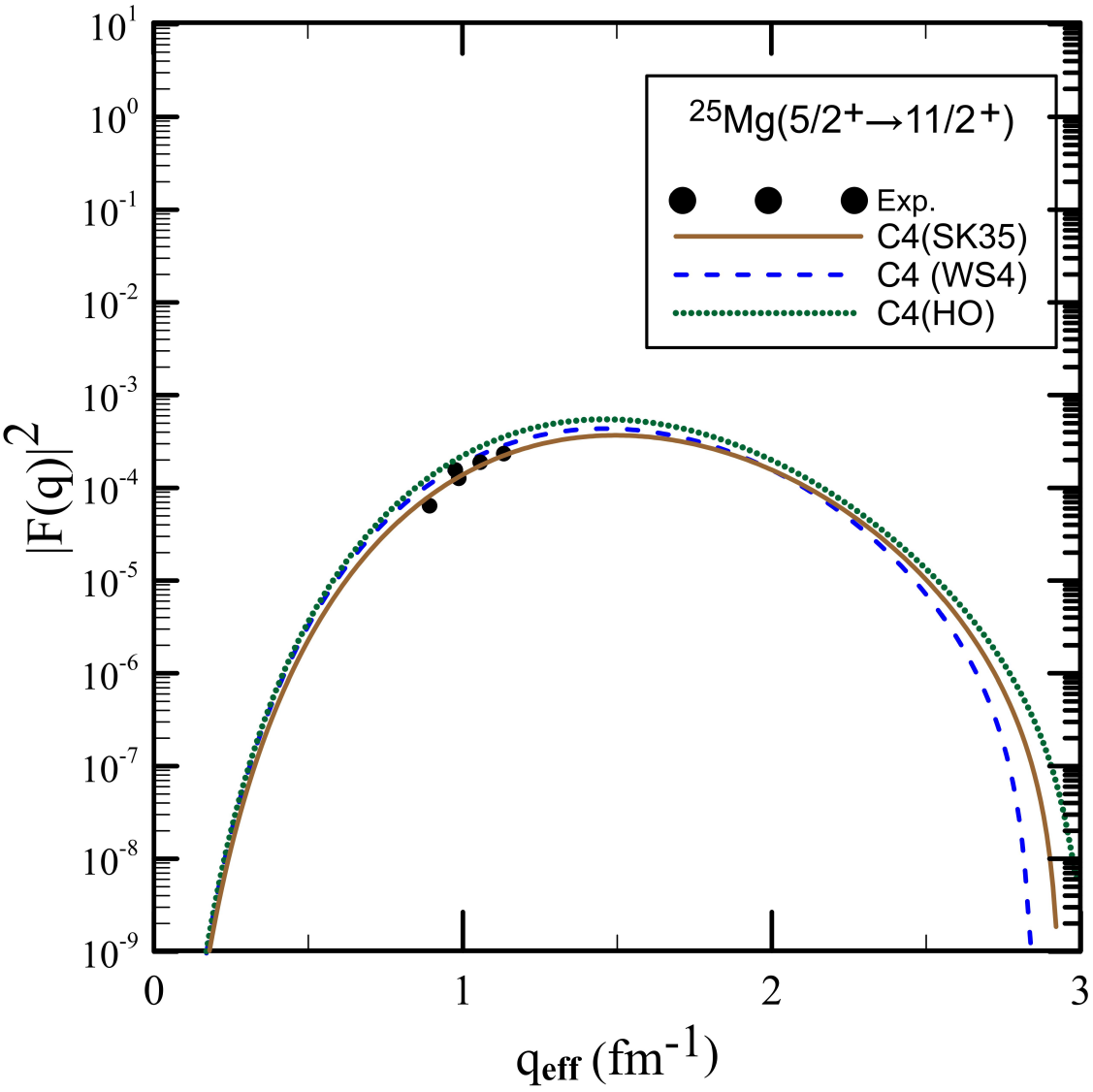

Figure 4.17: The relation between moment transfer q_{eff} and longitudinal C4 form factor $F(q)$ for ^{25}Mg nucleus. The curve represent the calculation Bohr-Mottelson (BM) collective model with SKX, WS, and HO potentials.

4.6 Conclusions

The present study focus on Bohr-Mottelson model to calculate the electron scattering form factors for some selected states of sdpf-shell nuclei, therefore we had concluded the following:

1. The sdpf-shells model space wave functions using the sdpfnow as residual effective interaction has succeeded in describing some states of ^{31}P, ^{27}Al, ^{23}Na and ^{24}Mg nuclei considered in this study.

2. An excellent agreement was obtained between the theoretical results and the experimental data by using the SKX potential capabilities that are better than those of WS and HO potentials of the ^{31}P nucleus.

3. The electron scattering form factor results of ^{31}P nucleus with HO potential shifted the calculations toward increased the momentum transfer on the second and third maximum momentum transfer region.

4. The calculations with HO potential agree with the experimental data for ^{23}Na nucleus but the calculations with WS and SKX potentials failed.

5. The longitudinal form factor calculations of ^{27}Al nucleus with SKX potential are better than WS and HO potentials in transition from ground state to $1/2_2$, but the results with WS potential is better than other potentials in transitions to $3/2_2$ and $7/2$, when compared the results with the experimental data.

6. When comparing result of ^{25}Mg nucleus with the experimental data, a good agreement is obtained when used the WS potential for transitions to $5/2_2$, $7/2$, $9/2$, and $9/2_2$ but for the transitions to $1/2_2$, $3/2_2$, and $11/2$ with SKX potential is better than other potentials.

7. The calculations with Harmonic Oscillation (HO), Wood-Saxons (WS) and Skyrme-Hartree Fock (SKX) potentials for radial part of the single-particle matrix elements are able to agree with the

practical results of ^{31}P and ^{23}Na nuclei and for some states of ^{27}Al and ^{25}Mg nuclei.

8. The Bohr-Mottelson (BM) collective model gives a good description of longitudinal form factor of some nuclei in C0, C2, and C4 transitions as compared with experimental data.

9. The calculations of BM collective model with SKX potential succeeded compared with WS and HO potentials to comply with practical values of ^{31}P nucleus and the states of ^{27}Al but some states ^{25}Mg.

4.7 Suggestions of Future Work

We suggest the following:

1. Extending this work in an attempt to include the other nuclei in the sdpf-shell.

2. This work can be repeated by considering no-core shell model calculations for the same nuclei and compare these calculations with the present work.

3. Extending this work in an attempt using some other residual effective interaction such as sdpfmw, sdpfwb, or sdpfwa.

References

[1] B. A. Brown. “The nuclear shell model towards the drip lines”. In: Progress in Particle and Nuclear Physics 47.2 (2001), pp. 517–599.

[2] Y. Utsuno, T. Otsuka, T. Mizusaki, and M. Honma “Varying shell gap and deformation in N 20 unstable nuclei studied by the Monte Carlo shell model”. In: Physical Review C 60.5 (1999), p. 054315.

[3] K. S. Krane and D. Halliday. “Introductory Nuclear Physics John Wiley & Sons”. In: Inc., Kanada (1988), p. 116-158.

[4] R. A. Radhi and A. Bouchebak. “Microscopic calculations of C2 and C4 form factors in sd-shell nuclei”. In: Nuclear Physics A 716(2003), pp. 87–99.

[5] O. Haxel, J. Hans D. Jensen, and H. E. Suess. “On the magic numbers in nuclear structure”. In: Physical Review 75.11 (1949), p. 1766.

[6] S. Mohammadi, E. Zare Morzi, and N. S. Shakib. “Energy Levels Calculations of Potassium Isotopes Using OXBASH Code”. In: International Journal of Scientific Engineering and Applied Science 2.11 (2016), pp. 72–75.

[7] M. H. Chen, B. Crasemann, and H. Mark. “Relativistic M-shell radiationless transitions”. In: Physical Review A 21.2 (1980), p. 449.

[8] A. Poves et al. “Shell model study of the isobaric chains A= 50, A= 51 and A= 52”. In: Nuclear Physics A 694.1-2 (2001), pp. 157–198.

[9] Z. Czyżewski, D. O'Neil, A. Romig, and D. C. Joy “Calculations of Mott scattering cross section”. In: Journal of Applied Physics 68.7 (1990), pp. 3066–3072.

[10] S. Raman, S. Raman, X. Ouyang, M. A. Islam, J. W. Starner, E. T. Jurney, and J. E. Lynn. "Thermal-neutron capture by ^{58}Ni,^{59} Ni, and ^{60}Ni". In: Physical Review C 70.4 (2004), p. 044318.

[11] K. S. Jassim. "Nuclear Structure of ^{104,106,108}Sn Isotopes Using the NuShell Computer Code". In: Chinese Journal of Physics 51.3 (2013), pp. 441–451.

[12] A. Yakhelef and A. Bouldjedri. "Shell model calculation for Te and Sn isotopes in the vicinity of ^{100}Sn". In: AIP Conference Proceedings 8. (2012), pp. 199– 203.

[13] J. D. Walecka. "Electron scattering for nuclear and nucleon structure". Vol. 16. Cambridge University Press, (2001). pp. 29-331.

[14] E. Caurier, F. Nowacki, A. Poves, and J. Retamosa "Shell model study of the neutron rich isotopes from oxygen to silicon". In: Physical Review C 58.4 (1998), p. 2033.

[15] S. S. Wong. "Introductory nuclear physics". John Wiley & Sons, (2008). pp. 21-102.

[16] P. Sarriguren, D. Merino, O. Moreno, E. Moya, D. N. Kadrev, A. N. Antonov, and M. K. Gaidrov "Elastic magnetic electron scattering from deformed nuclei". In: Physical Review C 99.3 (2019), p. 034325.

[17] R. R. Roy and B. P. Nigam. "Nuclear physics: theory and experiment". Wiley, (1967). pp. 22-201.

[18] K. Furukawa, M. Kabasawa, T. Kawamrura, Y. Takahashi, A. Satoh, T. Nakagawa, H. Orihara, T. Nizeki, K. Ishii, K. Maeda, K. Miura, B. A. Brown, and H. Ohnuma. "^{34}S(p, n)^{34}Cl reaction at 35 MeV and its microscopic distorted-wave Born approximation analysis: Stringent test of the shell model". In: Physical Review C 36.5 (1987), p. 1686.

[19] X. Roca-Maza. "Theoretical calculations for precision polarimetry based on Mott scattering". In: EPL (Europhysics Letters) 120.3 (2018), p. 33002.

[20] M. Honma, T. Otsuka, B. A. Brown, and T. Mizusaki "Effective interaction for pf-shell nuclei". In: Physical Review C 65.6 (2002), p. 061301.

[21] A. Bohr and B. R. Mottelson. “Rotational states in even-even nuclei”. In: Physical Review 90.4 (1953), p. 717.

[22] P. J. Brussaard and P. WM. Glademans. Shell-model Applicationin Nuclear Spectroscopy” North. (1977).

[23] A. A. Al-Saad. “Admixture of higher multi-ħωconfigurations in the calculation of electron scattering form factors of some 1p-shell nuclei”. In: Turkish Journal of Physics; Volume: 36 (2012). pp. 352-360.

[24] K. S. Jassim and H. A. Kassim. “Core Polarization effects of some odd sd-shell nuclei using M3Y effective nucleon-nucleon interaction”. In: Romanian Journal of Physics 58.3-4 (2013), PP. 319-29.

[25] N. M. Adeeb, A. A. Alzubadi, and O. A. Jalal. “Longitudinal and Transverse electron scattering form factors for ^{13}C nucleus with Core-Polarization effects”. In: Iraqi Journal of Science 54.4 (2013), pp. 888–894.

[26] R. A. Radhi, Z. A. Dakhil, and B. S. Hameed. “Elastic and inelastic magnetic electron scattering form factors of neutron-rich 19C exotic nucleus”. In: Iraqi Journal of Science 55.4B (2014), pp. 1859–1867.

[27] K. S. Jassim and Z. M. Abdul-Hamza. “Longitudinal (C2) form factors with core-polarization effects of some fp-shell nuclei using Tassie model.” In: Armenian Journal of Physics 7.4 (2014). pp. 166-176.

[28] F. A. Majeed and L. A. Najim. “Contribution of high energy configurations to longitudinal and transverse form factors in p and sd-shell nuclei”. In: Indian Journal of Physics 89.6 (2015), PP. 611-618.

[29] A. A. Al-Sammerraie, F. I. Sharred, N. Yusof, and H. Abu Kassim. “Longitudinal and transverse electron-nucleus scattering form factors of ^{25}Mg” . In: Physical Review C 92.3 (2015), P. 034327.

[30] J. Liu, X. Zhang, C. Xu, and Z. Ren. “Theoretical study on nuclear structure by the mul- tiple Coulomb scattering and magnetic scattering of relativistic electrons”. In: Nuclear physics A 948 (2016), PP. 46-62.

[31] K. S. Jassim and R. A. Abdul-Nabi. “Core-Polarization Effects on the Isoscalar and Isovector Transitions in ^{24}Mg Using Extended Shell Model”. In: Journal of Advanced Physics 5.4 (2016), pp. 349–353.

[32] K. S. Jassim and S. R. Sahib. “Large-Scale sdpf Shells model calculations for Electron scattering form factors and charge density distribution for the ^{19}F Nuclei”. In: Journal of Chemical and Pharmaceutical Sciences 10 (2017), pp. 1070–1074.

[33] J. Liu, J. Zhang, C. Xu, and Z. Ren. “Nuclear longitudinal form factors for axially deformed charge distributions expanded by nonorthogonal basis functions”. In: Chinese Physics C 41.5 (2017), p. 054101.

[34] T. Liang, J . Liu, Z. Ren, C. Xu, and S. Wang “Elastic electron scattering form factors of deformed exotic Xe isotopes”. In: Physical Review C 98.4 (2018), p. 044310.

[35] K. S. Jassim and S. R. Sahib. “Large-scale shell model calculations of the ^{25,26}Mg,^{27} Al and ^{19}F nucleus”. In: International Journal of Nuclear Energy Science and Technology 12.1 (2018), pp. 81–91.

[36] A. R. Ridha and Zaid M. Abbas. “Theoretical Study of density distributions and size radii of ^{8}B and ^{17}Ne”. In: Iraqi Journal of Science (2018), pp. 1046–1056.

[37] A. D. Salman, Samah A Al-Ramahi, and MH Oleiwi. “Inelastic electron-nucleus scattering form factors for ^{64,66,68}Zn isotopes”. In: AIP Conference Proceedings Vol. 2144. 1. AIP Publishing LLC. (2019), p. 030029.

[38] J. Liu, R. Xu, J. Zhang, C. Xu, and Z. Ren. “Elastic electron scattering off nuclei with shape co- existence”. In: Journal of Physics G: Nuclear and Particle Physics 46.5 (2019), p. 055105.

[39] P. Sarriguren, O. Moreno, E. Moya, D. N. Kadrev, A. N. Antonov, and M. K. Gaidarov “Elastic magnetic electron scattering from odd-A nuclei”. In: Journal of Physics: Conference Series. Vol. 1555. 1. IOP Publishing. (2020), p. 012001.

[40] A. K. Hasan, F. H. Obeed, and A. N. Rahim. “Positive parity levels of ^{21,23}Na Isotopes by using the nuclear shell”. In: Ukrainian Journal of Physics 65.1 (2020), pp. 3.

[41] H. M. Dlshad, A. Hama-Raheem Fatah, and A. M. Hussain. “The Elastic and inelastic electron-nucleus scattering form factors for ^{9}Be nucleus”. In: UHD Journal of Science and Technology 4.2 (2020), pp. 56–62.

[42] R. A. Radhi, A. A. Alzubadi, and N. S. Manie. “Electromagnetic multipoles of positive parity states in ^{27}Al by elastic and inelastic electron scattering”. In: Nuclear Physics A 1015 (2021), p. 122302.

[43] I. AH. Ajeel, M. JR. Aldhuhaibat, and K. S. Jassim. “Coulomb C2 and C4 Form Factors of ^{18}O,^{20,22} Ne Nuclei Using Bohr- Mottelson Collective Model”. In: Ukrainian Journal of Physics 67.2 (2022),pp. 110–110.

[44] J. D. Walecka. “Theoretical nuclear and subnuclear physics”. WorldScientific Publishing Company, (2004). pp. 115-201.

[45] K. Heyde and B. R. Barrett. “Basic Ideas and Concepts in Nuclear Physics: An Introductory Approach”. In: Physics Today 52.12 (1999), p. 60.

[46] B. A. Brown. “Lecture notes in nuclear structure physics”. In: National Super Conducting Cyclotron Laboratory 11 (2005).

[47] T. Dytrych, P. Maris, K. D. Launey, J. P. Draayer, J. P. Vary, D. Langer, E. Saule, M. A. Caprio, U. Catalyurek, and M. Sosonkina. “Efficacy of the SU (3) scheme for ab initio large- scale calculations beyond the lightest nuclei”. In: Computer Physics Communications 207 (2016), pp. 202–210.

[48] R. A. Radhi and E. A. Salman. “Collective E2 transitions in^{18}O”. In: Nuclear Physics A806.1-4 (2008)), pp. 179–190.

[49] M. Fabre De La Ripelle, S. A. Sofianos, and R. M. Adam. “Method for solving the many-body bound state nuclear problem”. In: Annals of Physics 316.1 (2005), pp. 107–159.

[50] C. B. Dover and N. Van Giai. “The nucleon-nucleus potential in the Hartree-Fock approximation with Skyrme’s interaction”. In: Nuclear Physics A 190.2 (1972), pp. 373–400.

[51] R. D. Woods and D. S. Saxon. “Diffuse surface optical model for nucleon-nuclei scattering”. In: Physical Review 95.2 (1954), p. 577.

[52] T. HR. Skyrme. “The effective nuclear potential”. In: Nuclear Physics 9.4 (1958), pp. 615–634.

[53] R. Machleidt. “Computational Nuclear Physics 2–Nuclear Reactions”. In: Langanke, Maruhn, Koonin, eds., Springer NY(1993). pp. 25-102.

[54] J. Lee, B. Tsang. “Neutron spectroscopic factors of ^{34}Ar and ^{46}Ar from (p, d) transfer reactions”. In: Physical Review C83.1 (2011),p. 014606.

[55] W. Greiner and J. A. Maruhn. Nuclear models. Springer, (1996). pp. 65-74.

[56] J. Rainwater. “Nuclear energy level argument for a spheroidal nuclear model”. In: Physical Review79.3 (1950)), p. 432.

[57] A. N. Bohr and B. R. Mottelson. Nuclear Structure (In 2 Volumes). World Scientific Publishing Company, (1998). pp. 200-315.

[58] A. Bohr, B. R. Mottelson, and G. Breit. “Nuclear structure, vol. 1”. In: Physics Today 23.9 (1970), p. 58.

[59] A. Bohr, B. R. Mottelson, G. Breit, and G. E. Brown. “Nuclear Structure, Vol. 2: Nuclear Deformations”. In: Physics Today 30.3 (1977), p. 59.

[60] D. L. Hill and J. A. Wheeler. “Nuclear constitution and the interpretation of fission phenomena”. In: Physical Review 89.5 (1953), p. 1102.

[61] J. M. Eisenberg and W. Greiner. “Nuclear theory”. In: (1987). pp. 123-200.

[62] A. Bohr. “Rotational motion in nuclei”. In: Reviews of Modern Physics 48.3 (1976), p. 365.

[63] L. Próchniak and S. G. Rohoziński. “Quadrupole collective states within the Bohr collective Hamiltonian”. In: Journal of Physics G: Nuclear and Particle Physics 36.12 (2009) p. 123101.

[64] G. Gneuss, U. Mosel, and W. Greiner. “A new treatment of the collective nuclear Hamiltonian”. In: Physics Letters B 30.6 (1969), pp. 397–399.

[65] B. Mottelson. “Elementary modes of excitation in the nucleus”. In: Reviews of Modern Physics 48.3 (1976), p. 375.

[66] T. de Forest Jr. and J. D. Walecka. “Electron scattering and nuclear structure”. In: Advances in Physics 15.57 (1966), pp. 1–109.

[67] T. William Donnelly and J. D. Walecka. “Electron scattering and nuclear structure”. In: Annual Review of Nuclear Science 25.1 (1975), pp. 329–405.

[68] H. Uberall and T. W. Donnelly. “Electron scattering from complex nuclei, parts A and B”. In: Physics Today 25.10 (1972), p. 45.

[69] N. F. Mott. “The scattering of fast electrons by atomic nuclei”. In: Proceedings of the Royal Society of London. Series A, Containing Papers of a Mathematical and Physical Character124.794 (1929), pp. 425–442.

[70] A. DeShalit and H. Feshbach “Theoretical nuclear physics. Volume I. Nuclear structure”. In: (1974).

[71] T-SH. Lee and D. Kurath. “Inelastic pion scattering for 1 p- shell targets”. In: Physical Review C 21.1 (1980), p. 293.

[72] L. J. Tassie. “A model of nuclear shape oscillations for g Transitions and electron excitation”. In: Australian Journal of physics 9.4 (1956), pp. 407–418.

[73] P. J. Brussaard and P. WM. Glaudemans: “Shell-Model Applications in Nuclear Spectroscopy”, North-Holland, Amsterdam and New York, (1977). In: 34.6 (1979), pp. 525–526.

[74] K. Langanke, D. J. Dean, P. B. Radha, Y. Alhassid, and S. E. Koonin. “Shell-model Monte Carlo studies of fp-shell nuclei”. In: Physical Review C 52.2 (1995), p. 718.

[75] K. Kaneko, Y. Sun, M. Hasegawa, and T. Mizusaki. “Structure of upper-$g_{9/2}$-shell nuclei and shape effect in the ^{94}Ag isomeric states”. In: Physical Review C 77.6 (2008), p. 064304.

[76] L. Jo Tassie and F. C. Barker. “Application to electron scattering of center of mass effects in the nuclear shell model”. In: Physical Review 111.3 (1958), p. 940.

[77] B. A. Brown, R. Radhi, and B. H. Wildenthal. “Electric quadrupole and hexadecupole nuclear excitations from the perspectives of electron scattering and modern shell-model theory”. In: Physics Re- ports 101.5 (1983), pp. 313–358.

[78] H. Uberall. Electron scattering from complex nuclei V36A. Academic Press, (2012). pp. 101-204.

[79] T. W. Donnelly and J. D. Walecka. "Elastic magnetic electron scattering and nuclear moments". In: Nuclear Physics A 201.1 (1973), pp. 81–106.

[80] A. N. Antonov, P. E. Hodgson, and I. Zh. Petkov. Nucleon Momentum and Density Distributions in Nuclei Clarendon. (1988).

[81] A. N. Antonov, I. S. Bonev, C. V. Christov, and I. Z. Petkov. "Generator coordinate calculations of nucleon momentum and density distributions in ^{4}He,^{16} O and ^{40}Ca". In: Il Nuovo Cimento A 100.5 (1988), pp. 779–788.

[82] B. A. Brown and W. DM. Rea. NUSHELL@MSU:MSUNSCL Report.(2007).

[83] J. Liu, C. Xu, S. Wang, and Z. Ren. "Coulomb form factors of odd-A nuclei within an ax- ially deformed relativistic mean-field model". In: Physical Review C 96.3 (2017), p. 034314.

[84] B. B. P. Sinha, G. A. Peterson, G. C. Li, and R. R. Whitney. "Nuclear charge distributions of isotone pairs. I. ^{31}P and ^{32}S". In: Physical Review C 6.5 (1972), P. 1657.

[85] N. J. Stone. "Table of nuclear magnetic dipole and electric quadrupole moments". In: Atomic Data and Nuclear Data Tables 90.1(2005), PP. 75-176.

[86] P. P. Singhal, A. Watt, and R. R. Whitehead. "Elastic electron scattering from ^{23}Na,^{25} Mg and ^{27}Al and a shell-model interpretation". In: Journal of Physics G: Nuclear Physics 8.8 (1982), p. 1059.

[87] R. P. Singhal, A. Johnston, W. A. Gillespie, E. W. Lees. "Inelastic scattering of electrons from ^{27}Al". In: Nuclear Physics A 279.1 (1977), pp. 29–44.

[88] E. W. Lees, C . S. Curran, T. E. Drake, W. A. Gillespie, A. Jonston, and R. P. Singhal. "Inelastic electron scattering from ^{25}Mg". In: Journal of Physics G: Nuclear Physics 2.5 (1976), p. 341.

الخلاصة

تم حساب عوامل التشكل الطولي لاستطارة الإلكترون لبعض النوى الخفيفة مثل ^{31}P و ^{23}Na و ^{27}Al و ^{25}Mg التي تقع في منطقة القشرة sdpf. تم أخذ نواة ^{16}O كقلب. تم إجراء حسابات انموذج القشرة بواسطة كود Nushell للحاسوب. اؤخذ تأثير استقطاب القلب في الاعتبار لجميع النوى.

تم استخدام نموذج بور- موتلسون (BM) الجماعي في الحساب عوامل التشكل لاستطارة الالكترون مع المتذبذب التوافقي (HO) و(WS) Wood-Saxon's و(SKX) Skyrme-Hartree كجهود.

تم استخدام فضاء sdpf مع التفاعل الفعال المتبقي sdpfnow لحساب القيمة الذاتية والمتجهات الذاتية المستخدمة في الحساب مصفوفة كثافة الجسم الواحدة (OBDM) لاستخدامها في حسابات استطارة الإلكترون غير المرن والمرن.

تمت مقارنة البيانات التجريبية مع البيانات المقدرة غير المرنة و المرنة لاستطارة الإلكترون للأنوية المدروسة. تأثيرات استقطاب القلب من خلال الشحنات الفعالة للبروتونات والنيوترونات تبين أنها مهمه للغاية، وتتفق مع الأدلة التجريبية لعوامل التشكل الكولومية C0 وC2 و C4 بشكل كبير. تتفق الحسابات مع HO كجهد مع البيانات التجريبية لنواة ^{23}Na و لكن الحسابات مع SKX و WS كجهود تتفق بشكل افضل من HO مع اللأنوية ^{31}P و ^{27}Al و ^{25}Mg.

جمهورية العراق
وزارة التعليم العــالي والبحث العلـمي
جامــعة بابـــــل
كليـة التربية للعلوم الصرفة
قسـم الفيزيـــاء

دراسة استطارة النواة – الكترون في فضاء الانموذج sdpf لبعض النوى المشوهة

رسالة مقدمة
إلى مجلس كلية التربية للعلوم الصرفة في جامعة بابل
وهي جزء من متطلبات نيل درجة الماجستير
في التربية/ الفيزياء

من قبل الطالب

محمد ليث عدنان محمد جواد
بكالوريوس في الفيزياء
جامعة بابل ٢٠١٩

بأشراف

أ. د. خالد صالح جاسم

كلية التربية للعلوم الصرفة /قسم الفيزياء

١٤٤٤ هـ ٢٠٢٢م